Tissue-mimicking phantom materials with tunable optical properties suitable for assessment of diffuse reflectance spectroscopy during electrosurgery

Amiri, Sara Azizian; van Berckel, Pieter; Lai, Marco; Dankelman, Jenny; Hendriks, Benno H.W.

DOI
10.1364/BOE.449637

Publication date
2022

Document Version
Final published version

Published in
Biomedical Optics Express

Research Article | Vol. 13, No. 5 / 1 May 2022 / Biomedical Optics Express 2616
Biomedical Optics EXPRESS

Tissue-mimicking phantom materials with tunable optical properties suitable for assessment of diffuse reflectance spectroscopy during electrosurgery

SARA AZIZIAN AMIRI,[1,*] PIETER VAN BERCKEL,[1] MARCO LAI,[2,3] JENNY DANKELMAN,[1] AND BENNO H. W. HENDRIKS[1,2]

[1]*Department of Biomechanical Engineering, Faculty of Mechanical, Maritime, and Materials Engineering, Delft University of Technology, The Netherlands*
[2]*Philips Research, IGT & US Devices and Systems Department, Eindhoven, The Netherlands*
[3]*Eindhoven University of Technology (TU/e), Eindhoven, The Netherlands*
[*]*s.azizianamiri@tudelft.nl*

Abstract: Emerging intraoperative tumor margin assessment techniques require the development of more complex and reliable organ phantoms to assess the performance of the technique before its translation into the clinic. In this work, electrically conductive tissue-mimicking materials (TMMs) based on fat, water and agar/gelatin were produced with tunable optical properties. The composition of the phantoms allowed for the assessment of tumor margins using diffuse reflectance spectroscopy, as the fat/water ratio served as a discriminating factor between the healthy and malignant tissue. Moreover, the possibility of using polyvinyl alcohol (PVA) or transglutaminase in combination with fat, water and gelatin for developing TMMs was studied. The diffuse spectral response of the developed phantom materials had a good match with the spectral response of porcine muscle and adipose tissue, as well as *in vitro* human breast tissue. Using the developed recipe, anatomically relevant heterogeneous breast phantoms representing the optical properties of different layers of the human breast were fabricated using 3D-printed molds. These TMMs can be used for further development of phantoms applicable for simulating the realistic breast conserving surgery workflow in order to evaluate the intraoperative optical-based tumor margin assessment techniques during electrosurgery.

1. Introduction

As the number of women diagnosed with breast cancer increases every year [1,2], the challenge of complete tumor resection and achieving a negative margin during breast-conserving surgery (BCS) needs to be addressed. BCS is the preferred type of surgical approach for treatment of the patients with early-stage breast cancer. During surgery, the surgeon intends to remove the tumor completely from the breast of the patient and meanwhile preserve the overall shape of the breast as much as possible by avoiding unnecessary healthy tissue removal [3]. By investigating the excised specimens after BCS, the pathologist confirms whether the tumor resection was complete (negative margin) or that some parts of the tumor remained inside the breast of the patient after surgery (positive margin). When detecting a positive margin, treatment of the patient may have to be followed by a re-excision surgery or boost radiation therapy [3–5]. The occurrence rate of re-excision surgery ranges from less than 10% to around 50% which would ultimately lead to negative cosmetic outcomes associated with less patient satisfaction after surgery or additional morbidity [6–11]. Detecting tumor margins and discriminating diseased tissue from healthy tissue without any direct feedback during BCS, is a bothersome challenge for the surgeon during BCS [12–14]. Although using a margin assessment technique may appear to be quite effective in detecting the border of the tumor in BCS, each of the currently available techniques bears its

#449637 https://doi.org/10.1364/BOE.449637
Journal © 2022 Received 29 Nov 2021; revised 8 Feb 2022; accepted 9 Feb 2022; published 4 Apr 2022

Biomedical Optics EXPRESS

limitations, so the challenge of finding an effective intraoperative tumor detecting technique still stands [8,15,16].

1.1. Diffuse reflectance spectroscopy

Diffuse reflectance spectroscopy (DRS) is a non-destructive optical technology that measures the concentration of constituents of the tissue, based on its special intrinsic absorption and scattering of light in each wavelength [17–19]. It has been shown that DRS has the potential to be used as a real-time tumor margin detection technique during breast cancer surgery. DRS enables discrimination of diseased- from healthy tissue in different organs based on the different tissue-light interactions that originate from the different tissue compositions [20–30]. The study of De Boer et al. on application of DRS for investigating the ex vivo lumpectomy specimens showed that using a threshold F/W-ratio, breast tumor tissue (with F/W-ratio lower than the determined threshold) can be distinguished from benign tissue (with F/W-ratio higher than the specified threshold) with a specificity and sensitivity of 100% when the tumor border sites are not included. The F/W-ratio of breast tissue varies from patient to patient, hence, a patient-specific F/W-ratio needs to be defined using the F/W-ratio of the healthy tissue as a Ref. [21]. Moreover, in another in vivo study, the F/W-ratio provided the most effective discrimination between the tumor and healthy tissue with the Area Under Curve (AUV) of 0.94 in a Receiver Operator Characteristic (ROC) analysis [20]. Furthermore, De Boer et al. also showed that among different classification methods, models developed based on the F/W-ratio (mean sensitivity: 0.71, mean specificity: 0.99), full-spectrum (mean sensitivity: 0.94, mean specificity: 0.89) and selected wavelengths (eight wavelengths, mean sensitivity: 0.95, mean specificity: 0.91) were of the most promising predictive models for distinguishing the breast malignant tissue from healthy tissue using DRS [24].

Since DRS is a promising tumor margin assessment technique, DRS can be integrated into common surgical instruments to provide surgeons with real-time and intraoperative feedback of the tissue. For the same purpose, we recently developed an electrosurgical knife integrated with DRS and showed the possibility of detecting the tissue type while cutting/coagulating it [31–33]. The developed prototype has been tested on ex vivo porcine adipose and muscle tissue, assuming those tissues represent human healthy and tumor breast tissue sufficiently [31–33]. However, to allow for a successful transition of the prototypes into the clinical phase, more precise validation and accurate assessments are needed. The application we are aiming for includes electrosurgery to excise specimens. Tissue mimicking materials (TMMs) can be developed to allow electrosurgery on them, and hence simulation of the workflow of the realistic breast conserving surgery (lumpectomy). In addition, these TMMs and phantoms can be developed to closely simulate the optical properties of the different layers of the breast tissue. The development of such TMMs could make it possible to form a well-controlled environment for the accurate evaluation of the DRS-integrated electrosurgical knife or, in general, other relevant optical-based margin assessment techniques during electrosurgery.

1.2. Breast phantoms

Nowadays, tissue-mimicking materials (TMM) and phantoms are a vital part of medical device development. Using a phantom enables accurate validation, optimization and calibration of the new device before its transition to clinical applications. Moreover, a realistic organ phantom can be useful for training medical residents and surgeons to employ the new surgical instrument or intraoperative imaging system in the workflow of the surgery [34,35]. Up to now, several phantoms have been developed by researchers for assessing the optical or spectral tissue sensing systems in clinical applications such as diffuse optical spectroscopy [34,36], fluorescence imaging [37,38] optical tomography [39–41], photoacoustic imaging [42,43] and also for the assessment

Biomedical Optics EXPRESS

of optical imaging systems in combination with other imaging techniques such as MRI [44] or ultrasound [45].

A realistic breast phantom enables simulation of the different properties of breasts layers as well as the surgical workflow of BCS. For such a realistic phantom the following requirements are defined:

1. Validation of DRS and DRS integrated in the electrosurgical knife, requires that the phantom represent realistic fat- and water percentages of different layers of the breast. As mentioned before, the amount of fat and water in healthy and tumor breasts tissue is a determinative factor for detecting these two tissues using DRS [21]. For instance, a phantom with different layers, same as human breast, each with a distinct F/W-ratio, could be very useful in evaluating the application of the DRS in tumor margin detection. Moreover, detection of the border of the tumor before actually reaching it can be easily and explicitly examined using a layered phantom.

2. To simulate realistic breast surgery, the TMM must be made such that it can be cut with an electrosurgical knife. During the electrosurgery, a radio frequency alternating current is used to induce oscillation of the ionized molecules inside the tissue, which subsequently converts into thermal energy leading to an increase of the local tissue temperature, and finally tissue rupture. Similar to human tissue, the TMM should have enough ions, or in other words, sufficient electrical conductivity [46,47].

3. The TMMs should not extensively melt during electrosurgery when exposed to high temperatures. During electrosurgery, depending on the settings and tissue properties, the tissue temperature quickly rises to temperatures higher than 100°C, which results in localized tissue cutting/coagulation [48]. The various compounds may melt excessively after exposure to this high temperature. The TMMs are expected not to melt but rather cut cleanly (burned) during electrosurgery, similar to human tissue.

4. The TMM is preferred to show realistic tissue effects such as burning and debris formation during electrosurgery.

5. To simulate the anatomy of the breast realistically, a stable TMM in a realistic breast shape and layer configuration is needed.

6. Encompass other properties such as the ease of manufacturing, shape- and property stability over time, and cost-effectiveness.

Among different types of TMMs, biological-based compositions fulfil these requirements better than non-biological-based compositions. For instance, it is challenging to find and produce polymeric TMMs that represent the optical properties of fat and water sufficiently while being electroconductive [49]. Using water-soluble components, such as gelatin and agar, enables the use of fat and water, which leads to the simulation of the realistic tissue composition and optical properties [36]. On the other hand, using polymers such as polyvinyl chloride (PVC), silicone, polyester and polyurethane makes it almost impossible or difficult to include biological fat and water. In this case, additives such as glass microsphere, carbon black, titanium dioxide (TiO_2), microspheres, aluminium oxide (Al_2O_3) and gold nanoshells are needed to reach the absorption and reduced scattering coefficient of human breast tissue [35,39,42,50–52]. The addition of large number of additives makes the production process more complex, expensive and time-consuming. Furthermore, closely simulating the absorption and reduced scattering coefficient of fat and water in a continuous wavelength range using these additives is challenging [35,39,42,50–52]. In some applications in which monitoring the tissue only requires measuring the optical response of the tissue in one or a few wavelengths, additives such as TiO2 can be used to closely simulate the

Biomedical Optics EXPRESS

absorption and/or scattering profile of the tissue at those specific wavelengths [43]. However, it has been shown that a continues full-spectrum (400–1600 nm) DRS measurement or at least DRS measurement in eight specific wavelengths are required for correct detection of the breast tumor tissue from healthy tissue (or estimate the F/W-ratio of the tissue) using DRS [22].

Besides, most polymers are not electroconductive, hence to make them conductive more additives are needed, which bears more effort and drawbacks [53]. Agar and gelatin have been used vastly in producing different tissues mimicking compositions and phantoms [54,55]. Both biopolymers are relatively cheap, easy to process and can easily form different shapes. In comparison to agar (with a melting point of around 85°C), gelatin has a lower melting temperature of around 35°C, which makes gelatin less suitable for a phantom meant for electrosurgical applications [35,50,56]. Moreover, it is possible to adjust the electrical conductivity of these two biopolymers using additives such as sodium chloride (NaCl) [57]. One disadvantage of using some hydrogels is the lower life span and durability due to reducing water content or bacterial invasion. However, by controlling the packaging process and storage temperature or using preservative additives such as ethylenediaminetetraacetic acid (EDTA) or sodium azide (NaN_3), the durability of the agar and gelatin-based phantoms can be expanded [35]. TMM such as gelatin and agar, enables the development of a solid phantom that resembles the fat- and water percentage of the healthy and malignant breast tissue [36,40,58,59].

1.3. Fat-water based phantoms for medical optics: mini-review

Water-lipid compositions are desirable for making phantoms due to having the main biological components of breast tissue and many other organs. Recently these types of phantoms became popular in evaluating microwave imaging systems, in which the determinative parameter in distinguishing tissues from each other is the dielectric characteristics of the tissue. In these phantoms, water is mixed with different lipids and oils such as Kerosene, safflower oil, glycerin and grape seed oil [60–68]. Water-lipid phantoms have also been used for other imaging techniques. For instance, Merritt et al. developed a series of phantoms consisting of water, soybean oil and Triton x-100, where water and soybean oil represented the absorption characteristics of breast's water and fat, whereas Triton x-100 functioned as an emulsifier for water and lipid. These phantoms were used with water percentages ranging from 30 to 100 percent, on which a quantitative analysis was performed and the potential of MRI and diffuse optical spectroscopy in receiving the fat and water signals were compared. A good correlation between the results of these two systems was found [44]. Michaelsen et al. developed different anthropomorphic water-lipid based breast phantoms using different lipids (butter, margarine, olive oil, canola, vegetable oil and lard) as well as different emulsifiers (guar gum, soy lecithin and borax). Ultimately, guar gum in combination with water and lard was the most promising combination for a successful phantom. Compositions with fat and water percentages from 15% to 85% were produced for simulating layers of the breast. The final phantom was breast shaped and included an adipose layer with 30% water and 70% lipid, a fibroglandular layer with 70% water and 30% lipid, and a tumor insertion with 80% water and 20% lipid. Near-infrared tomography measurement showed the water percentages ranged from 30% for the adipose layer to 73% for the tumor [40]. Quatrole et al. also developed phantoms based on distilled water and commercial pork fat either with or without emulsifiers, to assess the capability of diffuse reflectance spectroscopy to estimate the concentrations of the constituents. Agar and Triton-X were used as emulsifiers to produce phantoms with 30–70%, 50–50% and 70–30% fat-water concentrations. Among all the phantoms, the group which was made of 1% agar showed better stability for the whole range of F/W-ratios. However, handling agar as a thickener complicated the production process, as precise control over temperature and timing are required to secure the agar phantom formation. Using Triton-x enabled the formation of all F/W-ratios, nevertheless, Triton-x led to higher scattering properties than tissue and low phantom durability of around 2–3 hours [58]. Ohmae et al. established

Biomedical Optics EXPRESS

semi-solid phantoms using distilled water, soybean oil as lipid, soybean lecithin as an emulsifier and either agar or oil solidifying agent as a coagulant. In their research, agar was used for phantoms with 99%, 80% and 60% of water (oil-in-water) and an oil solidifying agent was used for phantoms with 40%, 20% and 5% of water. To assess the water-to-lipid volume fraction of the phantoms, a six-wavelength time-domain diffuse optical spectroscopy system was used to estimate the concentration of constituents and suitability of the phantoms for this purpose [36]. Recently, Bush et al. developed a recipe of a fat-water phantom with a fat fraction of 0%, 25%, 50%, 75% and 100% consisting of distilled water, agar, oil-soluble, sodium benzoate and peanut oil. They showed a good correlation between the fat fraction measured by MRI and the target values in the developed phantoms [59].

The challenge regarding the development of these phantoms is to achieve good stability and homogeneity as well as the desired absorption and scattering profile. In this research, we developed four different phantom material recipes to simulate the different layers of the breast phantom. To simulate the fat content of human breast tissue as close as possible, pure porcine fat or lard were used in all phantoms. Like human white adipose tissue which is made up of mostly lipids in the form of triglycerides, lard consists of 97.9% triglycerides. This resemblance in composition between lard and human adipose tissue, as well as the fact that lard is easily accessible, makes lard a great and competent material to represent human adipose tissue in phantoms [69].

For the phantoms, agar and gelatin were both used as emulsifiers for fat and water, as well as a coagulant to solidify and stabilize the phantoms. In comparison with agar, gelatin has low thermal stability which makes it less suitable for electrosurgery. Lately, blending of polyvinyl alcohol (PVA) and gelatin has gained attention since the final product of this combination exhibits improved properties that could not be obtained from each of these polymers alone [70–73]. For instance, Thangprasert et al. showed that combining PVA and gelatin to form a hybrid hydrogel led to an increase of the compressive stress and young's modulus of the final composition [74]. Therefore to increase the overall stability of the gelatin phantom, PVA was used in one of the four phantoms in combination with lard, water and gelatin. Additionally, in this research, we used transglutaminase (TG) to enzymatically cross-link the gelatin to improve its stability and gel strength. TG is vastly used in the food industry to crosslink the proteins in milk and meat. Crosslinking gelatin using TG, results in a hydrogel with promising characteristics for biomedical and tissue engineering applications [75–80].

In this paper, TMMs were designed to simulate the optical properties of different layers of the human breast such that electrical surgery can be performed on those. The ultimate goal of producing such TMMs and phantom is to use them for assessment of the capability of the DRS system in detecting the tumor border while using the electrosurgical knife to excise the tumor during the breast conserving surgery (lumpectomy). For this purpose, four groups of phantoms were produced, namely based on lard-water-agar (Agar phantom), lard-water-gelatin (Gelatin phantom), lard-water-gelatin-PVA (Gelatin-PVA phantom) and lard-water-gelatin-TG (Gelatin-TG phantom). To the best of the authors' knowledge, these are the first results reported on the combination of lard-water-gelatin with or without PVA and TG to produce a TMM and a phantom. Phantoms with different amounts of fat and water content were produced to simulate the breast's different layers and tumor tissue. Diffuse reflectance spectroscopy was used to characterize the phantom materials. Unlike other studies in this area, light in 1000nm–1600 nm wavelength was used to measure the spectral response and optical properties of the phantom materials, as it has been shown that fat and water have their main optical absorption in this wavelength range [19,81]. The effect of electrosurgery on the TMMs was inspected qualitatively and the stability of the TMMs over time was investigated. Eventually, using the phantom materials, anatomically relevant heterogeneous breast phantoms representing the physiological

Biomedical Optics EXPRESS

Table 1. Materials for producing phantoms.

	For all phantoms					Only for Agar Phantom	Only for Gelatin based phantom		
	Lard (ml)	Water (ml)	NaCl (g)	Sodium benzoate (g)	BS (g)	Agar (g)	For all Gelatin based phantoms	Only Gelatin-TG Phantom	Only Gelatin-PVA Phantom
							Gelatin (g) (15%)	TG 1 g /6 g Gelatin	PVA(g)
Adipose	60	40	0.4 (1%)	0.04 (0.1%)	-	1.2 (3%)	6 (15%)	1 g	4 (10%)
Gland	40	60	0.6 (1%)	0.06 (0.1%)	-	1.8 (3%)	9 (15%)	1.5	6 (10%)
Tumor	20	80	0.8 (1%)	0.08 (0.1%)	1.6 (2%)	2.4 (3%)	12 (15%)	2 g	8 (10%)

composition and optical properties of human breast tissue including a tumor were developed for further research.

2. Materials and methods

2.1. Phantom materials preparation

Four different phantoms were developed, an Agar-based, Gelatin-based, Gelatin-TG-based and Gelatin-PVA-based phantom. For each phantom, three different compositions of Adipose, Gland and Tumor were used that represent the different layers of the breast, namely the adipose-, fibroglandular- and tumor tissue layer, respectively. The F/W-ratio of the Adipose, Gland (fibroglandular) and Tumor layer was respectively 60–40%, 40–60% and 20–80%. Table 1 indicates the amount of each component to produce 100 ml of each layer. The steps for producing each phantom are summarized in Fig. 1. To make the phantoms, agar powder extracted from red algae (HL0106, Natural Spices) or bovine gelatin powder 250 Bloom (ES1477, Natural Spices) were used as emulsifier. Pure lard (without any additives), which was produced by melting the belly fat of the pig at a low temperature, was purchased (ready to use) from the online butcher shop (JP Puurvlees, Netherlands). Also, a gelling agent, distilled water, Sodium Benzoate (Sigma-Aldrich, USA) as a preservative agent, and Barium sulphate (BS) (Hinmeijer, Netherlands) as a tumor contrast agent for x-ray imaging were used. Moreover, NaCl (Jozo, Netherlands) was used as an additive to manipulate the electrical conductivity of the TMMs, which leads to the free movement of ions in the solution and improvement of the conductivity [82]. Different concertation of NaCl (from 0.1 to 10 wt%) has been used in developing Agar phantoms that could mimic the electrical conductivity of various tissues for studying the effect of background tissue on radiofrequency-induced heating [83]. NaCl with concertation of 1% (or close to 1%) has been used in different studies for producing hydrogel phantoms based on TX-150 or agar or gelatin or synthetic polymer to adjust the electrical conductivity to represent the electrical properties of for example breast or muscle tissue [84–87].

Briefly, to develop the Agar phantom, the melted lard (in volume unit) was added to the water (in volume) mixture containing all the other chemicals (in mass unit) at boiling temperature.

To produce the Gelatin based phantoms, the lard was added to the water mixture at 50 °C. The percentage of the agar, gelatin, NaCl, sodium benzoate, and barium sulphate were based on the volume of the water. Right after adding lard to the water mixture for all phantom materials, a creamy opaque mixture was formed. To produce the Gelatin-TG phantom, after adding the lard to the gelatin-water mixture, the TG was added to it very slowly while the mixture was on the

Biomedical Optics EXPRESS

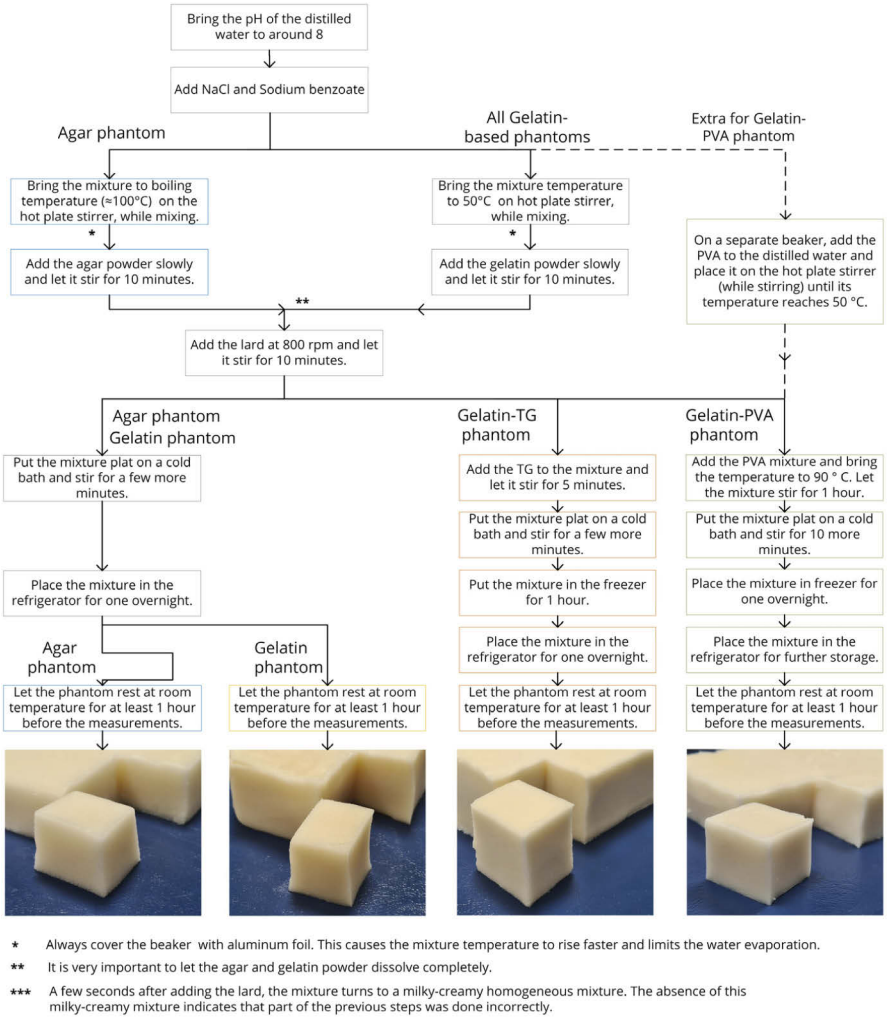

Fig. 1. Steps involved in producing four different phantoms.

stirrer. The Agar, Gelatin and Gelatin-TG phantoms were stored in the freezer for 1 hour and then refrigerated overnight. For the Gelatin-PVA phantom, a PVA-water mixture (PVA 10% g/ml.) was prepared beforehand and placed on a heater stirrer until the temperature reached 50 °C. Then the PVA mixture was added to the gelatin –lard water mixture and followed by staying on heater stirrer at 90 °C for one hour. Then the Gelatin-PVA mixture was stored in the freezer overnight and after that refrigerated. All phantom materials were produced in three replicates (three different batches). Before carrying out any assessment, all phantoms were taken out of the refrigerator and stayed at room temperature for 1 hour.

2.2. DRS measurements

To investigate the optical properties of the phantom materials and validate their application for DRS measurement, a Philips custom-designed diffuse reflectance spectroscopy setup (Philips Research, Eindhoven) was used. The device includes a halogen broadband light source (Avantes, The Netherlands) and a spectrometer designated to collect the light in the 900–1700nm spectral range (NIRQuest 512, Ocean Optics, USA). A flat-tipped optical needle consisting of two optical

Biomedical Optics EXPRESS

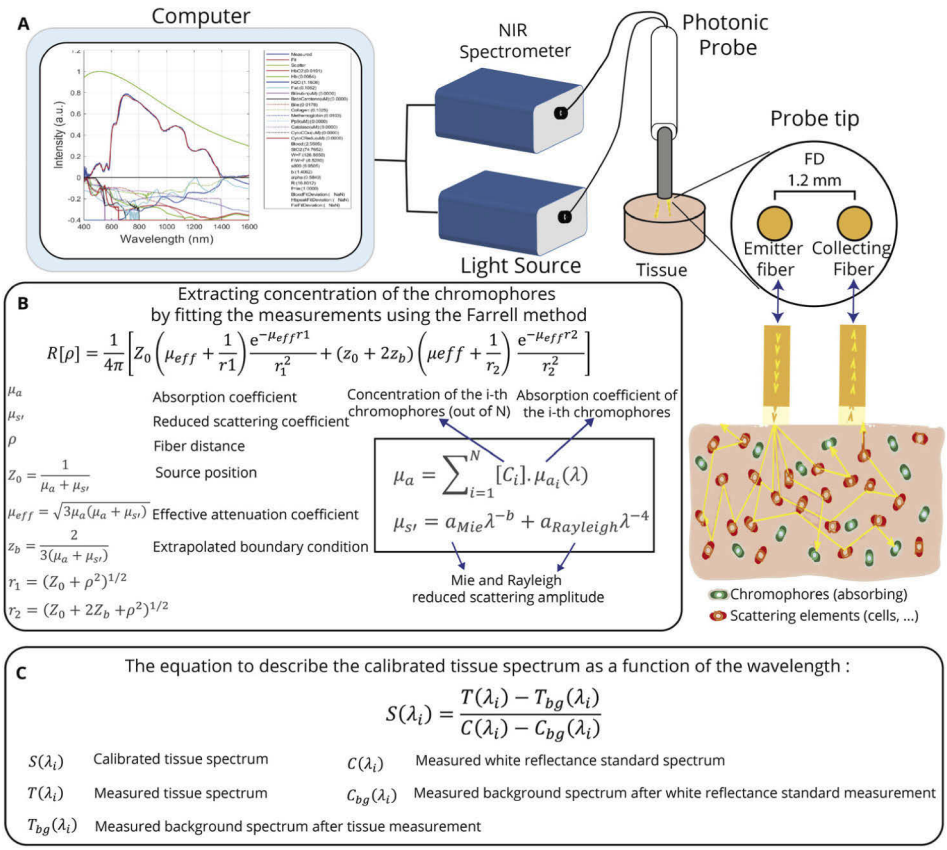

Fig. 2. (A) Custom-designed diffuse reflectance spectroscopy setup (made available by Philips). (B) Analytical models to translate the DRS measurements and calculate the concentration of the physiological parameters [90]. (C) Data pre-processing for calibration of the DRS system to compute the tissue spectrum from the measured and the calibration spectra [18,90].

fibers (with a total diameter of 220 µm, core diameter of 200 µm and numerical aperture (NA) of 0.22) with orientation parallel to the axis of the needle probe (end of the optical fibers are perpendicular to the probe axis) and a center-to-center fiber distance (FD) of 1.2 mm (fiber distance, FD), was used to emit the light from the light source to the tissue and collect the light to the spectrometer [31–33]. The setup used in this experiment is shown in Fig. 2(A). The measurements of the spectrometer were used as inputs for a Philips custom-developed Matlab-based software. In this software, the spectra were fitted with an analytical model, as explained in Fig. 2(B) which has first been described by Farrell et al. [88], by applying a nonlinear Levenberg–Marquardt inversion algorithm and subsequently the concentration of the chromophores were extracted from the fitted data [18,23]. More information regarding the design and application of diffuse reflectance spectroscopy can be found in these publications [17–19,23,89].

Calibration was carried out for the DRS setup, to minimize the effect of ambient light and emending the system response. For this purpose, using a probe-holder, the tip of the photonic needle was fixed on a 2 mm distance from a white reflectance standard (Spectralon with reflectivity of 99% for 400–1500 nm and >96% for 250–2000nm, model:WS-1-SL, Labsphere Inc., USA) (the distal end of the fibers were parallel to the standard). A 2 mm distance from the Spectralon

Biomedical Optics EXPRESS

was shown to provide sufficient accuracy for the DRS measurements (data not shown). Then the calibration was followed by measuring the spectral response of the white reference along with a background measurement [17,18,23]. In more detail, first, an inner wavelength calibration was performed on the sensor array of the detector to assign a wavelength to each pixel. Then the white reflectance measurements were performed (in front of the Spectralon) to measure the system response, and those were used later to offset the spectral shape of the light from the lamp as well as any wavelength-dependent sensitivity in the detector or optics of the system. Then to diminish the effect of the ambient light, a background measurement was performed. Moreover, each tissue/phantom measurement was followed by a background measurement by shuttering the light input. Eventually, the final tissue spectrum was defined using the equations mentioned in Fig. 2(C) as a function of the wavelength [18].

All the phantom/tissue measurements were obtained by placing the tip of the needle probe (optical fibers) at the distal end parallel and in contact with the TMMs and tissues. From each phantom material, three different locations were chosen randomly and from each location, three DRS spectra were obtained (produces nine spectra per phantom material). The fitted spectra of each measurement were calculated by using the software and consisted of the absorption profile, reduced scattering profile and concentration of chromophores. The extracted optical parameters for each spectrum are the total amount of fat and water (fat + water) and the fat fraction. Using the fat + water and fat fraction, the percentage of fat as Fat% and the percentage of water as Water% and F/W-ratio were calculated [21].

Moreover, the DRS measurements from human in vitro breast tissue reported by [91] was used in this paper to compare the characteristics of the TMMs with the targeted human tissue. These data had been taken from freshly excised breast tissue from normal fat, glandular, fibroadenoma lesions and (pre)-malignant locations.

Furthermore, as porcine adipose and muscle tissue own almost similar F/W-ratio as healthy and tumor breast tissue respectively [32,33], the spectral measurement from the two porcine tissues were used as a reference to relate the phantom spectral results to real breast tissue.

2.3. Electrosurgery

To study the effects of electrosurgery on the phantom materials, an electrosurgical knife with a blade shape electrode (WEIDE, Hangzhou Valued Medtech Co.,Ltd, China) connected to an electrosurgical unit (Force FX, Valleylab, Medtronic plc, USA) was used, as well as a dispersive pad. The knife was applied to each phantom material in the blend mode with 60 W power setting. To qualitatively compare the effects of electrosurgery on phantom tissue with the real tissue, porcine adipose and muscle tissue were used to simulate breast healthy and tumor tissue, respectively.

2.4. Stability over time

To investigate the stability of the phantom materials over time, DRS measurements were carried out on the phantoms after 10 days after the production day. During these 10 days the phantoms were stored in the refrigerator (4° C). Moreover, visual inspection was performed 3 weeks after the production day to check the morphological stability of the phantom materials over time.

2.5. Breast phantom preparation

The process of shaping the breast phantom was inspired by the work of Dantuma et al. [43]. To prepare the breast phantoms, three phantom materials with the best results were chosen (the reason will be discussed later). One 3D printed mold in the shape of a human breast and another 3D printed mold to form the fibroglandular layer were made, using the design of the models used in Ref. [43,92,93], as shown later in a figure. Silicone molds were made to produce tumors in different shapes and sizes. Following the process of realistic heterogeneous phantoms production

Biomedical Optics EXPRESS

in, first, the inner wall of the main breast mold was filled with a thin layer of silicone rubber (Dragon Skin 10 MEDIUM, Smooth-On, Inc.). This silicone layer allows the final phantom to be easily detached from the mold. In addition, silicone rubber can be dyed with skin-like colors to visually simulate the skin layer. Then the mold was filled with the adipose mixture while the fibroglandular mold was inserted inside it. The mold was stored in the freezer and after 1 hour the fibroglandular mold was removed carefully. In this way, the adipose layer was formed with a fibroglandular cavity in it. Tumors were made by filling the silicone molds with the tumor materials and letting the tumors rest in the freezer for 1 hour. To complete the phantom, tumors were fixed inside the fibroglandular layer cavity using wires and supports to hold those in the right positions. The gland mixture was poured inside the cavity and the whole phantom was stored in the freezer for 1 hour. Afterwards, the phantom was taken out, the wires were pulled out and the phantom was separated from the mold, and finally the phantoms were stored in the refrigerator overnight. Moreover, to inspect the visual similarity between the layers of the phantom, a layered phantom consisting of Tumor, Gland and Adipose layer was made using the Gelatin-TG TMMs.

2.6. X-ray validation

Three phantoms were made for the X-ray imaging. The X-ray imaging was performed using the Allura system (Philips Healthcare, Best, The Netherlands). With this system a 3D reconstructed volume with 0.5-mm voxel size of the phantoms was created.

2.7. Statistical analysis

For all the layers in each phantom, three replicates were made separately, which resulted in three Adipose, Gland and Tumor phantoms materials for each of the four different phantoms. For DRS measurements for each phantom material, three measurements were taken at three different locations of the phantom. To show the results of the spectra (DRS, absorption and reduced scattering), the mean spectra ± SD (standard deviation) for each phantom material (results of nine spectra for each phantom material) was used in the figures. For DRS measurements, before calculating the mean, all the spectra were first normalized. To study the significance of the data, t-test was used considering P values lower than 0.05 as significant. For all the statistical data analysis, GraphPad Prism version 8.1.2 (GraphPad Software, La Jolla, CA USA, www.graphpad.com) was used.

3. Results

Three different mixtures of phantom materials were produced, namely Adipose with 60% fat-40% water, Gland (representing fibroglandular layer) with 40% fat-60% water and Tumor with 20% fat and 80% water (percentage based on the total amount of fat and water). All phantom materials were stable when separated from the plate/mold and there was no sign of phase separation in the form of layers or particles. All phantoms were assessed on day 1 of production, after removing them from the refrigerator and letting them rest for 1 hour at room temperature. First, DRS measurements were carried out followed by electrosurgery and finally x-ray imaging was performed.

3.1. DRS measurements

The results of the DRS measurements of the phantom materials can be found in Fig. 3. The normalized spectra for each material are the mean spectra ± SD of all measurements from different locations of each replicates. Moreover, Fig. 4 shows the absorption and reduced scattering coefficients of each material. In Fig. 3 and 4. six wavelengths are marked with dotted lines. These marks indicate the wavelengths in which fat (blue dotted lines) and water (orange dotted lines) have their main absorption peaks.

Biomedical Optics EXPRESS

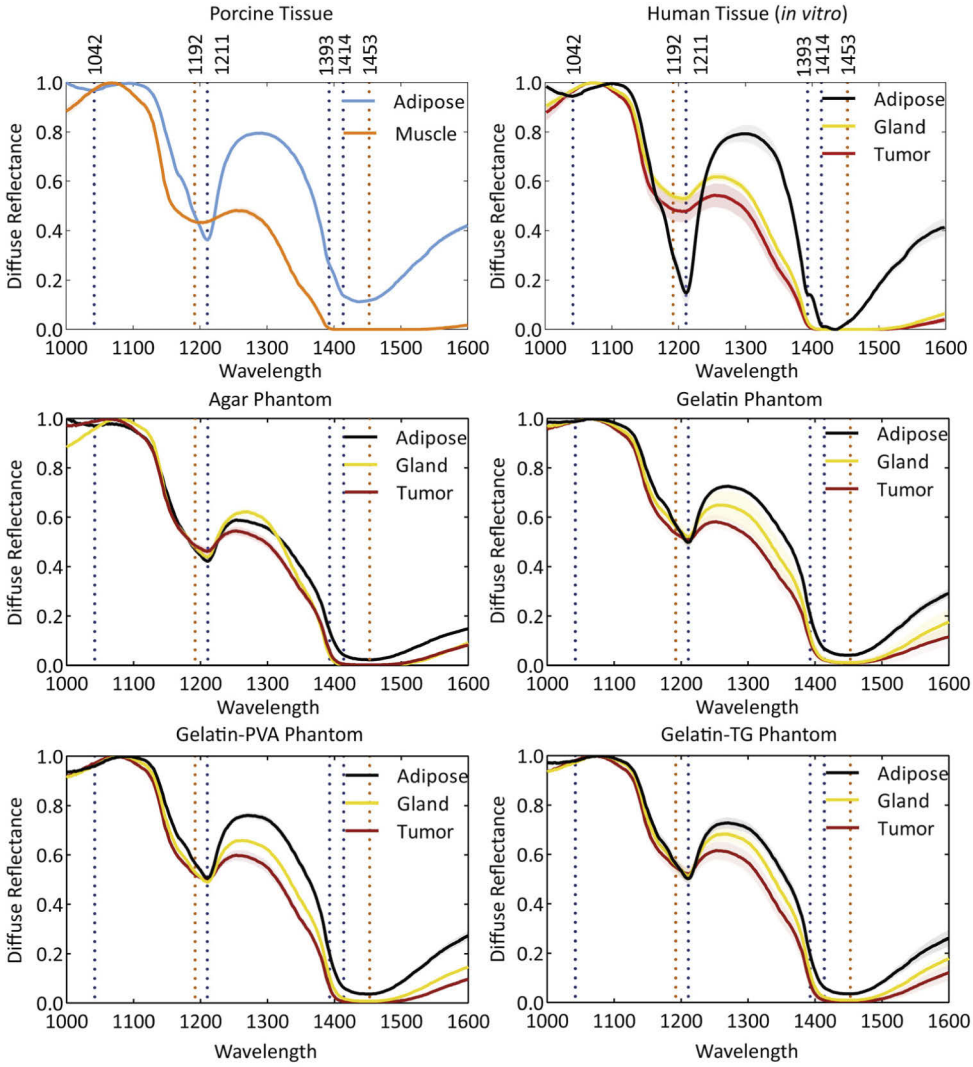

Fig. 3. DRS measurements taken from porcine tissue, human breast tissue from four different phantoms. The DRS data of human breast tissue is adapted from [91].

In Fig. 3 and 4, the DRS spectra of the fresh porcine adipose and muscle tissue as well as different types of *in vitro* human tissue (adapted from [91]) are visible. In Fig. 3 top boxes, the spectrum of the porcine adipose tissue (which simulates the breast adipose tissue) and human adipose tissue, show a sharp dent on 1211 nm and a flat dent between 1393 nm−1453 nm. The absorption coefficients of both human and porcine adipose in Fig. 4 displays a peak at 1211 nm and a flat and higher peak between 1400 nm and 1500 nm as well. On the contrary, the human tumor tissue (red) and porcine muscle spectrum shows a wider flat dent close to 1200 nm and becomes almost zero at 1400 nm and onward. In Fig. 4, the absorption of the human tumor tissue and porcine muscle shows a lower flat peak at 1200 nm area and a very high and sharp peak at 1453 nm, which corresponds to water absorption. As shown in Fig. 4, reduced scattering of all adipose tissues (human and porcine) is higher than reduced scattering of muscle (porcine) or tumor (human) tissue in all wavelengths.

Biomedical Optics EXPRESS

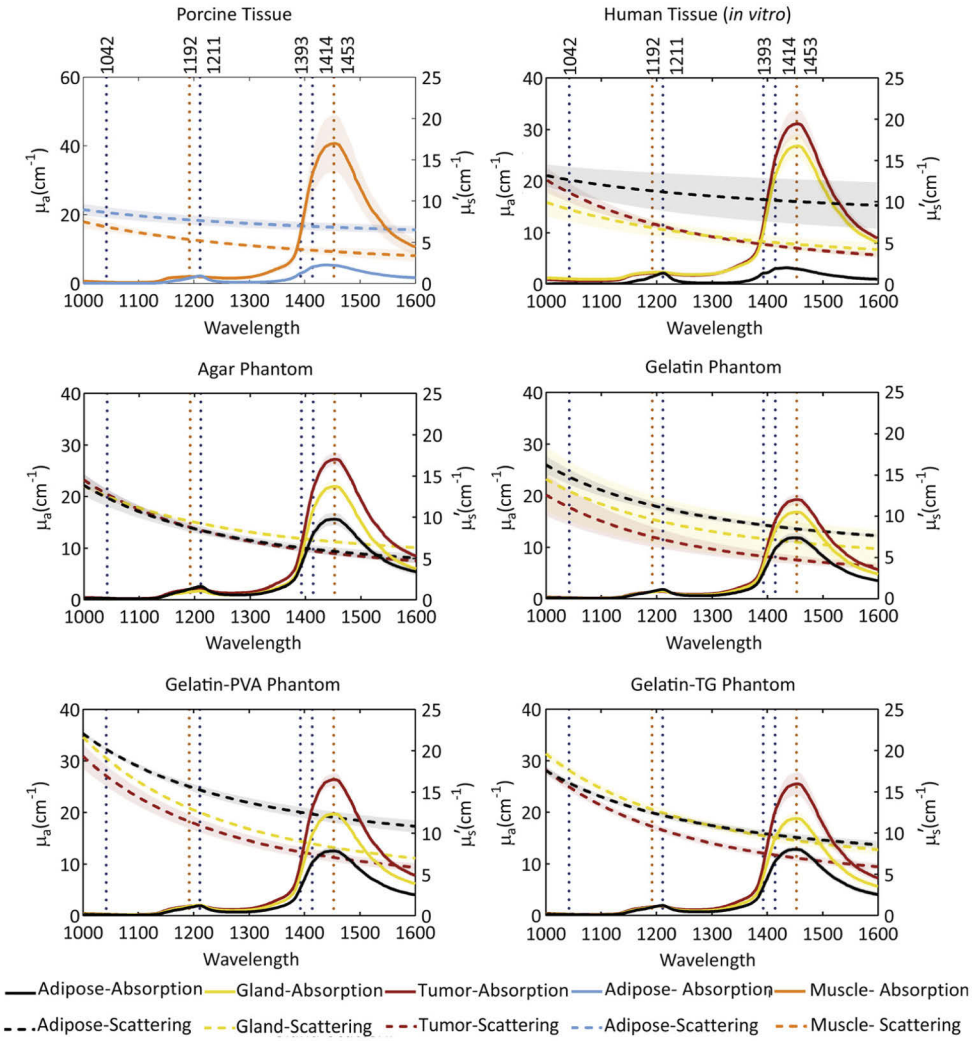

Fig. 4. Absorption (μa, cm-1) and reduced scattering (μ_s', cm^{-1}) coefficient of porcine tissue, human tissue (*in vitro*) and each tissue mimicking materials. The DRS data of human breast tissue is derived from [89].

The DRS spectra of all Adipose phantoms show one sharp dent around 1200 nm (at 1211 nm) and one flat dent around 1400 nm. Furthermore, the intensity remains more than zero in all wavelengths (same as porcine adipose tissue). Meanwhile, the absorption profile of the Adipose phantoms shows the same lower sharp peak on 1211 nm as well as the higher flatter peak between 1400 nm and 1500 nm, same as the porcine adipose tissue and human in vitro adipose tissue.

Like porcine muscle and human tumor tissue, the DRS spectra of the Tumor phantom shows flat dents around 1200 nm and 1400 nm (almost zero). The absorption profile of the Tumor phantoms also represents the same flat peak around 1200 nm and a sharp peak on 1453 nm, the same as muscle tissue (porcine) and tumor tissue (*in vitro*, human).

In between, all the Gland phantoms show DRS spectra similar to the spectra of the human *in vitro* gland. The Gland spectra for all TMMs and *in vitro* human tissue is between the spectra of the Adipose and Tumor phantoms with DRS dents not as sharp as Adipose tissue and not as

Biomedical Optics EXPRESS

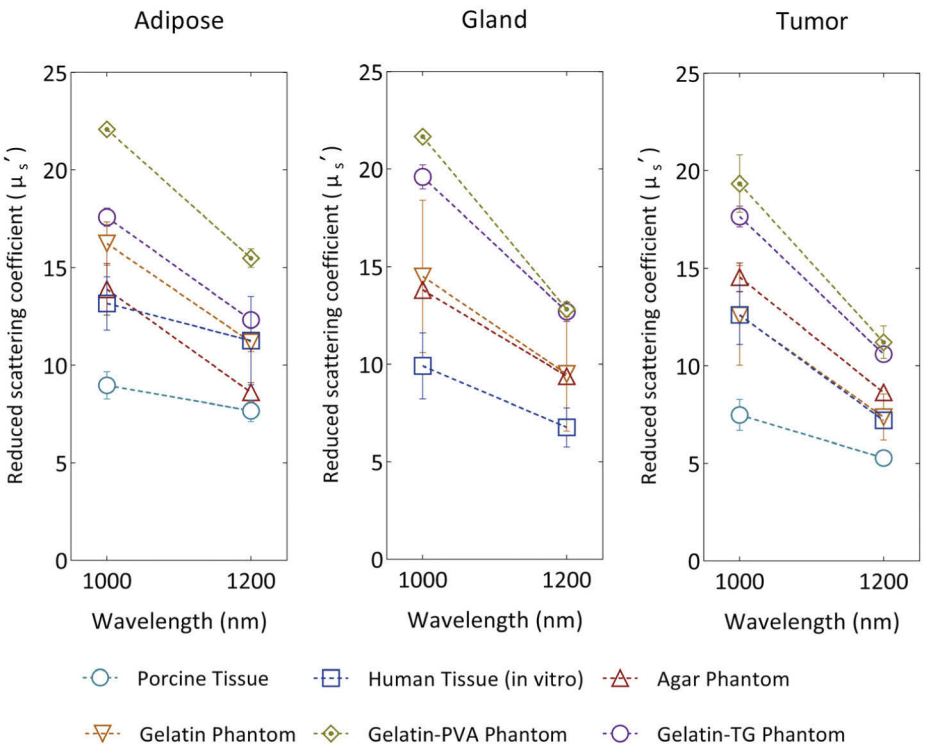

Fig. 5. Reduced scattering (μ_s', cm^{-1}) at 1000 nm and 1200 nm for porcine tissue, in vitro human breast tissue and each. TMMs.

Table 2. Reduced scattering coefficient (μ_s', cm^{-1}) at 1000 nm and 1200 nm.

	Type of the tissue					
	Adipose		Gland (fibroglandular tissue)		Tumor	
	1000 nm	*1200 nm*	*1000 nm*	*1200 nm*	*1000 nm*	*1200 nm*
Porcine tissue	8.96 ± 0.71	7.67 ± 0.56	-		7.48 ± 0.79	5.28 ± 0.09
Human tissue (*in vitro*)	13.17 ± 1.37	11.26 ± 2.26	9.91 ± 1.70	6.76 ± 0.99	12.61 ± 1.51	7.20 ± 0.38
Agar Phantom	13.88 ± 1.32	8.60 ± 0.50	13.81 ± 0.31	9.39 ± 0.20	14.53 ± 0.73	8.62 ± 0.30
Gelatin Phantom	16.23 ± 1.11	11.18 ± 0.48	14.49 ± 3.90	9.49 ± 2.92	12.58 ± 2.56	7.37 ± 1.18
Gelatin-PVA Phantom	22.07 ± 0.26	15.48 ± 0.47	21.65 ± 0.34	12.81 ± 0.06	19.33 ± 1.47	11.21 ± 0.84
Gelatin-TG phantom	17.58 ± 0.46	12.31 ± 0.33	19.60 ± 0.61	12.69 ± 0.50	17.66 ± 0.53	10.60 ± 0.41

flat as Tumor tissue. The spectra of Agar phantoms in Fig. 4 indicate similar reduced scattering for Adipose, Gland and Tumor tissue. For the Gelatin and Gelatin-PVA phantom, the reduced scattering of the Adipose phantom is higher than Tumor and reduced scattering of the Gland is in between those. For the Gelatin-TG phantom, the Adipose and Gland reduced scattering is almost

Biomedical Optics EXPRESS

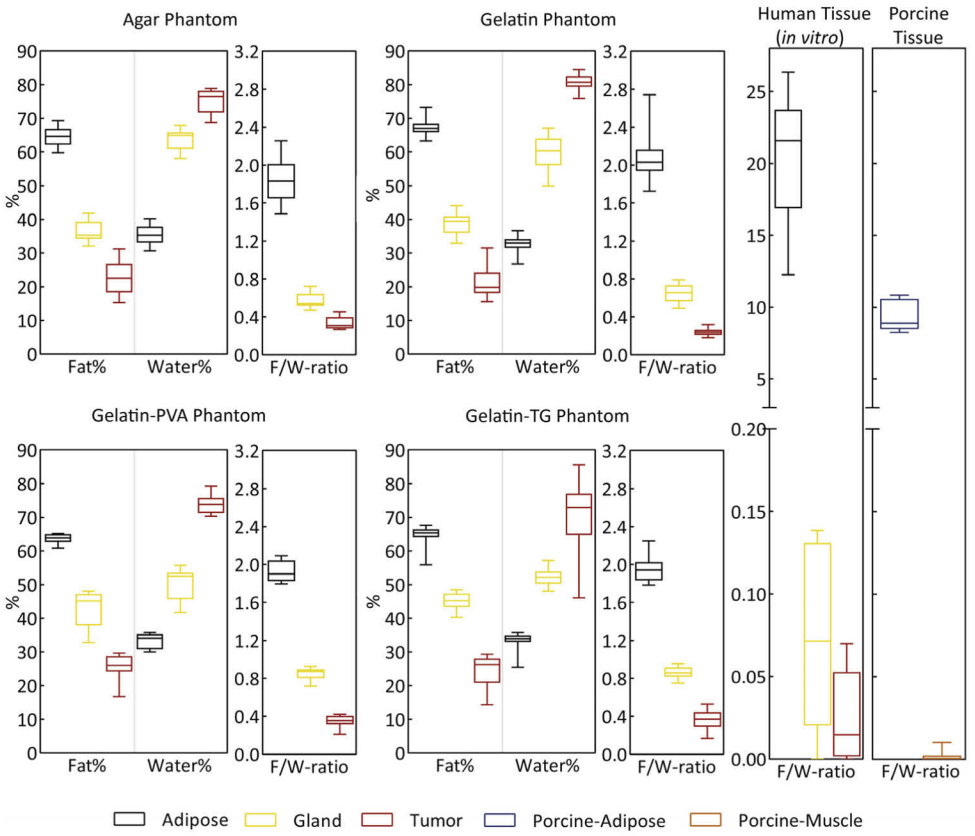

Fig. 6. The Fat%, Water% and calculated F/W-ration for each phantom extracted from the DRS measurements, boxes showing the min to max of the parameter along with its mean value (line inside the box).

the same after 1200 nm. The overall absorption and reduced scattering of the Gelatin phantoms are less than other phantoms.

In general Gelatin-PVA phantoms seem to have a lower SD which shows that the phantoms are more homogenous, also within a phantom (different locations) as well as between phantoms replicates. The absorption spectra of all Tumor phantoms show a lower peak in 1453 nm in comparison with the muscle tissue and *in vitro* human Tumor tissue. In addition, the height of the absorption peaks of the Adipose phantoms is close to the human adipose tissue, as well as those reduced scattering. In Table 2 and Fig. 5, the reduced scattering coefficients of porcine tissue, human *in vitro* samples and each TMM at 1000 nm and 1200 nm wavelength are listed. The reduced scattering of human adipose tissue has higher deviations ranging from around 10 to 15 cm^{-1}. Agar adipose phantom has the closest reduced scattering to the human adipose tissue at 1000 nm and to the porcine adipose tissue at 1200 nm, in comparison to other phantoms. On the other hand, at 1200 nm, Gelatin and Gelatin-TG adipose tissue simulate the reduced scattering of the human adipose tissue more closely. Moreover, Tumor mimicking material of Agar and Gelatin phantom also showed almost the same reduced scattering coefficient as the human tumor tissue and porcine muscle tissue. Adding PVA and TG to the Gelatin phantom resulted in higher reduced scattering numbers. The reduced scattering of both phantoms at 1000 nm are higher than the reduced scattering of human tissue but in higher wavelengths, such as 1200 nm, the reduced scattering of these phantoms get closer to the targeted human tissue.

Biomedical Optics EXPRESS

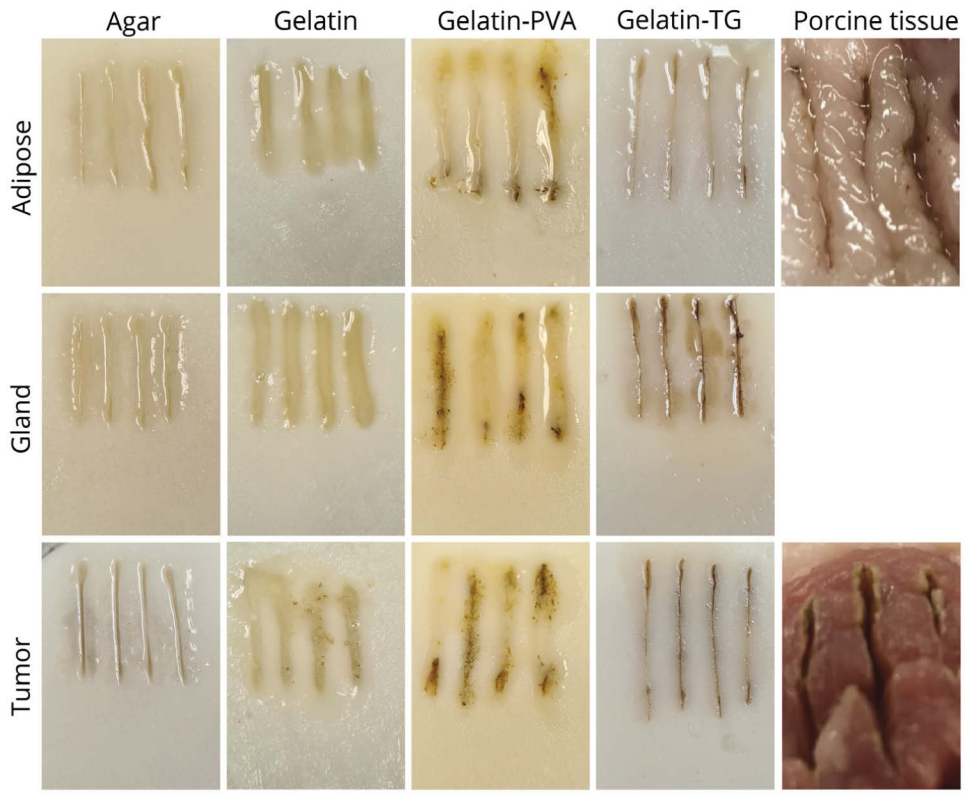

Fig. 7. The effect of electrosurgery on the tissue phantoms.

By using the software mentioned before, the fraction of fat and water was extracted from the DRS measurements for all phantom materials and subsequently, the F/W-ratio was calculated, as shown in Fig. 6. The float box plots in Fig. 6 show the mean, minimum and maximum of the Fat%, Water% and F/W-ratio. For all Adipose phantom materials, the Fat% is higher than 60%. The Fat% for the Gelatin-PVA phantom has the closest minimum to maximum, so the boxplot became smaller. Fat percentages among the Adipose, Gland and Tumor phantom materials of all phantoms have no overlap. This applies also to Water% and Fat/Water-ratio. From all the Adipose phantoms containing gelatin, the Adipose Gelatin phantom shows the highest Fat% and F/W-ratio. All phantoms show a clear distance between the F/W-ratios of the different layers

3.2. Electrosurgery

One hour after removing the phantom materials from the fridge, they were cut with the electrosurgical knife using 60 W. Figure 7 displays the pictures taken from each phantom after being cut. Similarly, to porcine adipose and muscle tissue, melting and burning occurred when cutting the phantoms with the electrosurgical knife. The Adipose phantoms and porcine adipose tissue showed the most melting whilst the Tumor phantoms and porcine muscle tissue showed the least melting. Among the phantoms, Gelatin and Gelatin-PVA melted the most and Gelatin-TG melted the least. Burning effects and char production were clearly visible on the Gelatin-PVA and Gelatin-TG phantoms. From the phantoms, the Adipose Gelatin-PVA and Adipose Gelatin-TG resembled the electrosurgical effects (melting and burning) to the porcine adipose tissue the most. Finally, cuttings on the Tumor Agar and Tumor Gelatin-TG phantoms were most similar to cuttings on the porcine muscle tissue.

Biomedical Optics EXPRESS

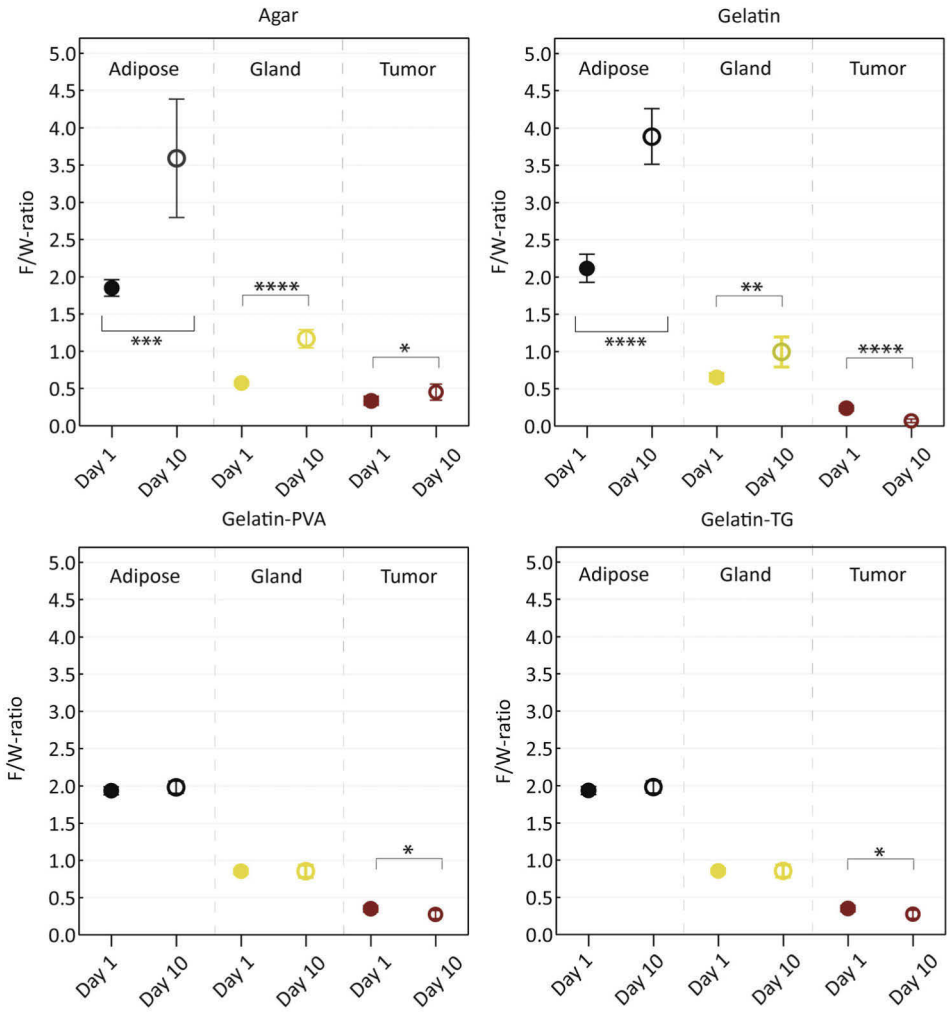

Fig. 8. F/W-ratio between the phantoms on day 1 and day 10 from the production (*: p-value < 0.05, **:p-value < 0.01, ***:p-value < 0.001, and ****: p-value < 0.0001).

3.3. Stability over time

To investigate how the phantom composition and optical properties would change over time, DRS measurements were carried out on all phantoms on day 10 after production. The F/W-ratio of all phantoms at day 1 and day 10 are shown in Fig. 8. The F/W-ratios for most phantoms increased after 10 days. The difference between the F/W-ratio at day 1 and day 10 for all Agar phantom and Gelatin phantom materials were significant. For Gelatin-PVA and Gelatin-TG there was not a significant difference between the F/W-ratio of day 1 and day 10 of the Adipose layers and Gland layers, while for the Tumor phantom the difference with one star was seen. Although time significantly changes F/W-ratios of most phantoms, there is still a significant difference in F/W-ratio between the Adipose, Gland and Tumor phantom materials (none of the phantoms' F/W-ratios overlap).

Additionally, a visual inspection of the phantom materials after three weeks was carried out. All Agar phantoms and Gelatin-PVA phantoms (different layers in replicates) were intact, there was no sign of mold or size reduction. On the other hand, small mold colonies were formed on

Biomedical Optics EXPRESS

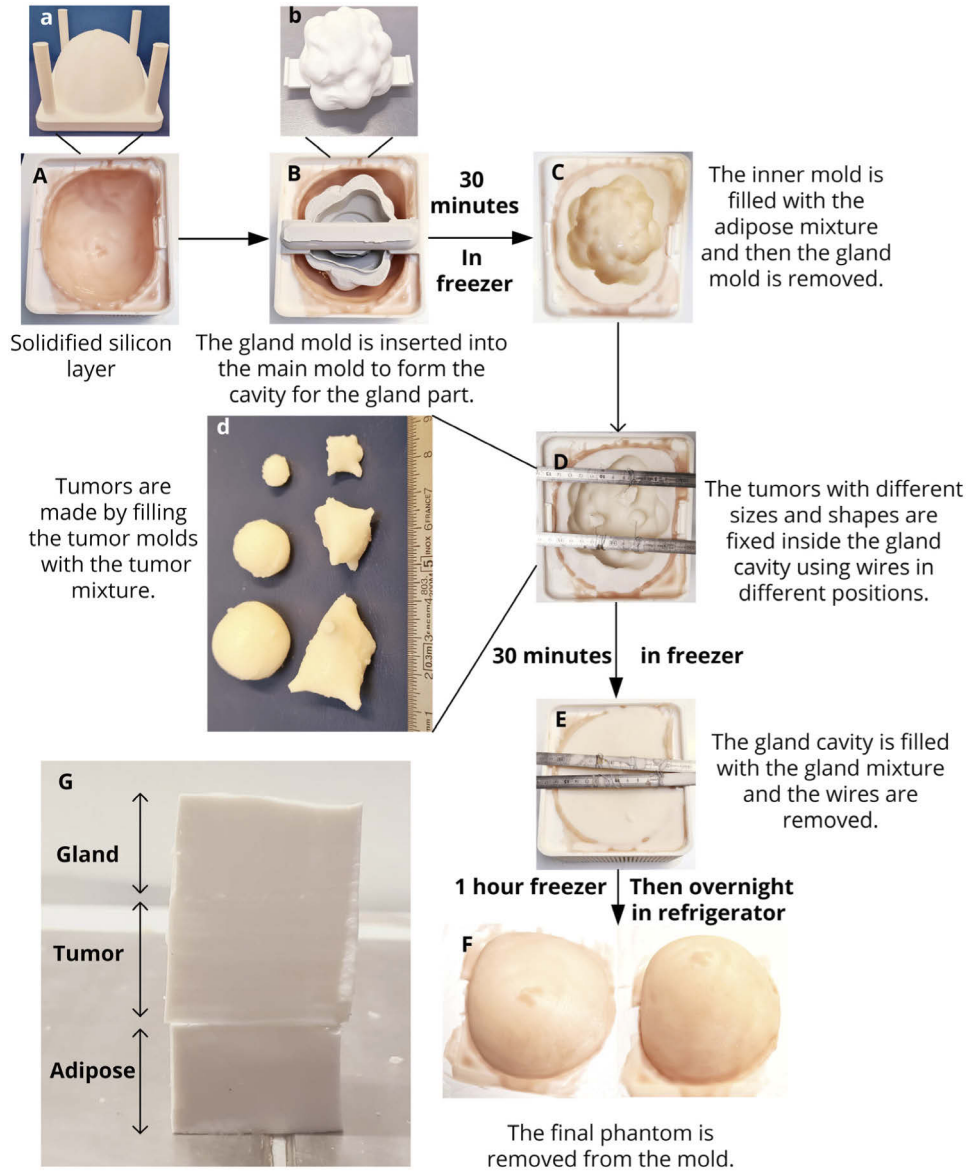

Fig. 9. (A-F) Production of the final breast phantom. (G) The layered phantom consists of Gland, Tumor and Adipose layers.

the surfaces of the Gelatin phantoms without any change in the size of the phantoms. Finally, concerning the Gelatin-TG phantoms, deformation occurred, and molds were formed all over the phantoms.

3.4. Breast phantom production

The breast phantoms were made following the production steps mentioned in Fig. 9. Using the silicone molds, it was possible to produce tumors in different shapes (with round edges or star-like shapes) and sizes (with a diameter of 0.5 cm to 4 cm) (Fig. 9(D)). After removing the gland mold (Fig. 9(B)), visible in Fig. 9(C), the gland cavity was made and then along with the tumors in it,

Biomedical Optics EXPRESS

it was filled with gland materials (Fig. 9(E)). In the end, a realistic breast phantom containing tumors in different shapes and sizes were produced (Fig. 9(F)). The presence of the silicone layer allowed the easy detachment of the phantom from the mold. Moreover, the silicone layer was colored with a skin-like silicone-based color to represent the appearance of the skin layer (only visually, no optical characterization has been done on the silicone layer). In further studies, this layer can be removed from the phantom if needed. Moreover, Fig. 9(G) shows a layered phantom with layers of Gland, Tumor and Adipose (respectively from top to bottom) made of Gelatin-TG TMMs. These layers have similar colors and textures, and distinguishing them from each other is challenging with the unaided eye. Considering the DRS and electrosurgical results, the Gelatin phantom was removed from the list of final phantom production as this phantom showed less suitable properties (less optical homogeneity, higher melting, and less stability over time) in comparison to other phantoms.

3.5. X-ray image of the phantoms

X-ray images were taken using the Allura system (Philips Healthcare, Best, The Netherlands) from the three chosen final breast phantoms (Agar phantom, Gelatin-PVA phantom and Gelatin-TG phantom). Figure 10 shows the side and top view of the phantoms as well as its 3D rendering with the inserted tumors. The images show successful insertion of the tumors and other layers of the phantoms. In all phantoms, the tumors were clear and visible due to the addition of the barium

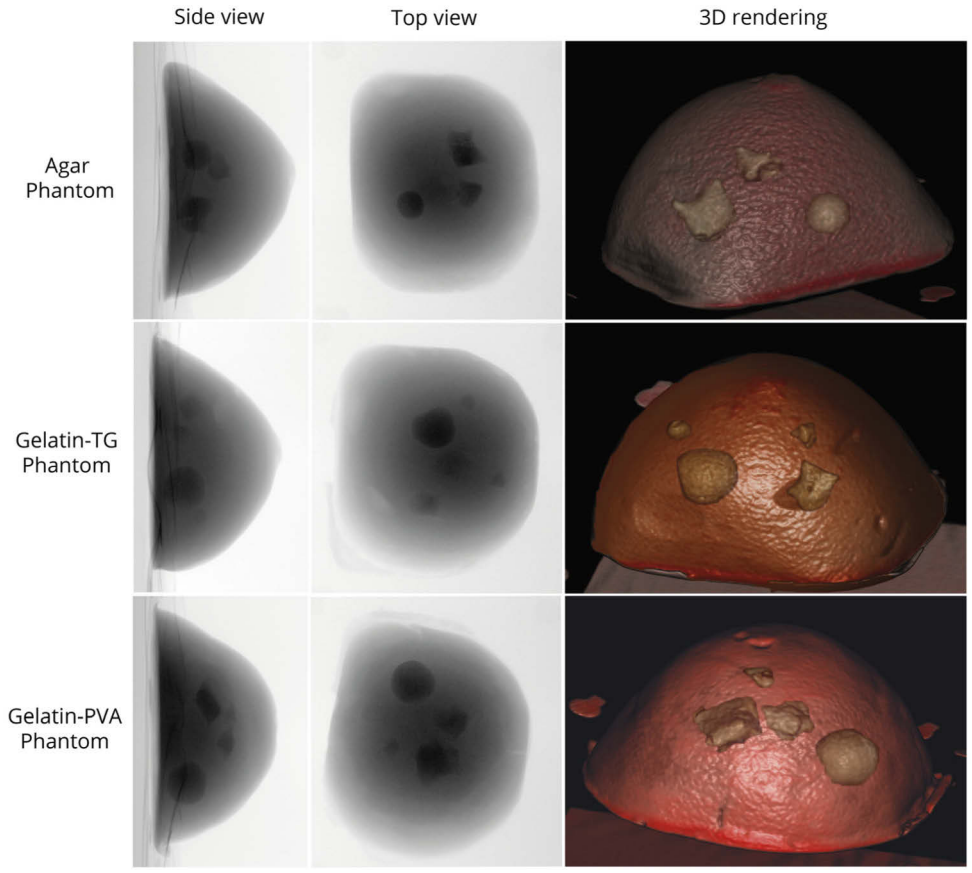

Fig. 10. X-ray images of the final phantoms.

Biomedical Optics EXPRESS

sulfate. The gland and adipose layer of the Gelatin-PVA phantom are clearly distinguishable from each other due to the difference in color, namely a darker color for the gland layer and a light grey color for the adipose layer. For the two other phantoms, the gland layer is only a little bit darker than the adipose layer but a clear margin for this layer is not visible.

4. Discussion

Fat-water based tissue-mimicking materials (TMM) and phantoms based on gelatin or agar with different recipes were developed in this work. The main purpose of developing such phantoms is to simulate the physiological composition of human breasts in different layers including tumors to assess the capability of the optical imaging systems, namely diffuse reflectance spectroscopy, in detecting the tumor during breast conserving surgery. To achieve this objective, phantoms were produced that represent the optical properties of the different layers of human breasts by controlling the amount of the lipid and water of the TMM as the main constituent of human tissue, specifically, women breast tissue. Agar and gelatin were used as a fat and water emulsifier as well as a gelling and coagulant agent to solidify the mixture. Additionally, the effect of adding polyvinyl alcohol (PVA) (Gelatin-PVA phantom) and transglutaminase (Gelatin-TG phantom) to the optical properties of the TMM and its stability during electrosurgery were investigated. The development process of all phantoms was time and cost-efficient and all the produced phantoms were stable at room temperature and easily moldable.

The results of the DRS measurements showed that the main absorption and reduced scattering profile of each TMM was similar to the target tissue. De Boer et al. investigated the spectral profile of different locations on sixteen specimens of lumpectomy samples to find the robust discriminative parameter between healthy tissue and tumor tissue in the NIR part using DRS [21]. They showed that for all samples, the F/W-ratio of all healthy locations was higher than a certain threshold, while for all tumor locations this parameter was lower than the threshold. Moreover, in almost all samples the F/W-ratio clearly decreased when moving from the healthy tissue to the border of the tumor tissue. They showed that by using a threshold for the F/W-ratio, it is possible to make a safe surgical plan to remove the tumor from the breast of the patient using DRS as an intra-operative margin assessment technique. This patient-specific F/W-ratio threshold, can be measured at the beginning of the surgery [21].

In another research, De Boer et al. also studied the effectiveness of DRS in an *in vivo* setup using a biopsy needle integrated with DRS optical fibers [24]. They showed that classification of the measurements based on F/W-ratio, results in healthy-tumor discrimination with mean sensitivity and specificity of 0.71 and 0.99, respectively. They could also classify the tissues correctly with high sensitivity and specificity (more than 0.91) using DRS measurements in some specific wavelengths. These specific wavelengths are in the wavelength range that is related to the main absorption of fat and water. These specific wavelengths are mostly in the range of 1000–1600 and that is why this wavelength range is used in this research, as the amount of fat and water is the main discriminating parameter between the malignant and healthy tissue of the breast. Moreover, at the surgical site blood contamination can decrease the reliability of the measurements at the visible part of the spectra (400–800) [24].

It has been shown that using a higher wavelength range of spectra can result in more precise tissue classification [21,24]. From the calculated Fat%, Water% and F/W-ratio of the produced TMMs (shown in Fig. 6) it is possible to consider a clear F/W-ratio threshold not only between the adipose and fibroglandular layer, but also between the tumor layer and both adipose and fibroglandular layer for all phantoms. Furthermore, the shape of the DRS spectra of the TMMs produced in Fig. 3 indicate a close similarity in the shape of the spectra between the TMM and its targeted *in vitro* human tissue and porcine tissue. Indeed, the shape of the spectra of the TMMs in this work is in accordance with the spectra of the healthy and tumor tissue of the breast measured by De Boer et al. [22,24]. The developed TMMs in this work could closely

Biomedical Optics EXPRESS

simulate the absorption and scattering profile of the human breast tissue. Therefore, similar to the human breast tissue [21], we can find a specific F/W-ratio that can be used as a threshold for discriminating healthy tissue phantom material (adipose and fibroglandular layer) from malignant tissue phantom material (tumor layer). Thereupon, we can create a surgical plan to detect the border of the tumor using DRS and remove it from the heterogeneous breast phantom using the electrosurgical knife.

Among all phantoms, Agar phantoms had a scattering profile closer to human breast tissue at 1000 nm while at 1200 nm, Gelatin-phantoms could represent reduced scattering coefficient closer to the human breast tissue. Taroni et al. showed reduced scattering close to 10 cm^{-1} for the breast tissue [94]. Yoshizawa et al. showed that breast tissue has reduced scattering between 5–15 cm^{-1} at 795 nm [95]. Moreover, Nachabe et al. showed that in the breast the reduced scattering amplitude at 800 nm is around 5 to 10 cm^{-1} depending on the type of the tissue [23]. De Boer et al. also determined that the reduced scattering at 800 nm for breast tissue (normal and malignant) ranges from around 5 cm^{-1} to 60 cm^{-1} [21]. Furthermore, Evers et al. measured reduced scattering from less than 5 cm^{-1} to around 20 cm^{-1} for different tissue of the breast at 800 nm [91]. In this research the approximate reduced scattering for all phantoms are in the range of 10 to around 20 cm^{-1} at 1000 nm, which is in accordance with Taroni et al. [94] and De Boer et al. [21] and the mentioned measurements form work of Evers et al. [91] in which a higher wavelength range was used to measure the spectral response of the human breast tissue. The reduced scattering profile of the Gland and Tumor layer is similar to the reduced scattering profile of the porcine muscle tissue and *in vitro* human adipose tissue. Besides, the slight differences between the DRS spectra of the Adipose layer and the porcine adipose tissue can be due to the lower amount of fat in the Adipose layer (60% fat) than the porcine adipose tissue (more than 90% fat). The reduced scattering of the Gland phantoms for all the composition is not matching exactly with the reduced scattering of the fibroglandular layer of human in vitro tissue which is due to the fact that the Fat% of the human fibroglandular tissue is lower than 40% (Fig. 6). Accordingly, reaching to the same scattering of fibroglandular layers is easily possible through adjusting the amount of the fat of the Gland layer of the TMM materials. Another point to consider regarding the optical properties of the developed TMMs is the effect that the addition of the barium sulfate (as an X-ray contrast agent) might have on the DRS outputs of the Tumor phantoms. The application of Barium Sulfate (BaSO4) as a reflection standard, due to its high reflectivity (average of 92%) in the range of 173–2500 nm, have been extensively studied [96]. It is known that the Mie reduced scattering slope (in equations explained in Fig. 2(B)) correlates with the particle size. Adding barium sulfate to the mixture can change the average particle size of the mixture and subsequently is reduced scattering [90,96]. Most of the barium sulfate containing Tumor TMMs developed in this research (more specifically Agar and Gelatin phantom) could closely simulate the reduced scattering coefficient of the human breast tumor tissue in higher wavelengths (1000 nm and 1200 nm). The F/W-ratio of the tumor phantoms were also in the expected range based on the production recipe in which fat and water were used with the ratio of 20:80 (20 ml fat, 80 ml water). However, understanding the extent to which the addition of the barium sulfate can affect the reduced scattering coefficient and the measured F/W-ratio of the material can be the subject of further studies.

Performing electrosurgery on all phantom materials was possible, and based on the qualitative inspections, TMMs showed similar effects as electrosurgery on porcine tissue. Adank et al. [31] showed that the coagulated area produced by cutting porcine tissue with the electrosurgical knife can alter the characteristics and affect the optical properties of porcine tissue. In their research, they showed that by increasing the power of the electrosurgical knife, reduced scattering will increase which results in overestimation of the fat fraction. To simulate realistic BCS for assessing spectral sensing systems such as DRS, it is required to consider the same electrosurgical effects for the phantoms materials. Among all phantoms, electrosurgery on the Gelatin phantom

Biomedical Optics EXPRESS

showed the least similarity in electrosurgical tissue effects (melting and burning) compared to the porcine tissue, which is due to the unstable character of gelatin in high temperatures. Among the other phantoms, the Gelatin-TG phantom resembled the electrosurgical tissue effects of porcine tissue the best. While all phantoms demonstrated electrosurgical tissue effects sufficiently similar to porcine tissue, more DRS studies are required to quantify the electrosurgical effects on the phantoms so that the electrosurgical tissue effects can be more accurately simulated in the future. Although producing a visually tissue-like electrosurgery effect was achievable using the developed TMMs, further studies are required to quantify this similarity. In an in-depth evaluation of the electrosurgery effect on TMMs, DRS spectra can be taken from the intact and then affected sites (cut or coagulated tissue) of phantom and *ex vivo* animal or human tissue. The results can then be compared to determine the quantitative similarity between the TMMs and human/porcine tissue regarding the electrosurgery effect.

It is also important to note that although the TMMs were produced to be used in electrosurgery applications, this research does not focus on the extent to which the TMMs can be quantitatively similar to human/porcine tissue in terms of electrical conductivity. The majority of these phantoms are used in the process of assessment and calibration of the detecting/imaging systems that work based on the electrical characteristics of the tissue, such as impedance spectroscopy and microwave imaging systems [97,98]. Due to the similar composition of the TMMs and breast tissue (both contain mostly fat and water), it is expected that these TMMs could (be modified to) have electrical properties similar to the human tissue. To show this, more comprehensive and quantitative assessment of the dielectric characteristics of the TMM is required, especially when they are intended for the applications in which measuring electrical properties of the TMMs are desired. In comparison to the other phantoms, DRS measurements of Gelatin-PVA and Gelatin-TG showed superior stability after 10 days of production. Concerning PVA, it has been shown that the physical crosslinking of the gelatin-PVA mixture can improve the mechanical properties of the final hydrogel [74]. Furthermore, Liu et al. showed that adding gelatin to PVA has no significant effect on the thermal behavior of PVA. This explains why adding PVA to the gelatin phantom (Gelatin-PVA) did not affect the electrosurgical effect of it, namely melting rather than burning effects were seen on the material [72]. Additionally, enzymatic crosslinking of gelatin using TG can increase the thermal stability and mechanical properties of the final product [99], which clarifies the decrease in melting of the phantom material with electrosurgery and the improved electrosurgical effect of the Gelatin-TG phantom in comparison to the Gelatin-Phantom.

It is noteworthy that the enzymatic crosslinking of gelatin in the Gelatin-TG phantom inhibits the water loss and increases the water detention and stability of the phantom, which is consistent with the results of other studies [100]. More research could be done in this area to measure the exact amount of water loss for each phantom. The increase of the F/W-ratio in the Agar and Gelatin phantom is due to the water loss after 10 days. Because of the increased cross-linked network of the Gelatin-PVA and Gelatin-TG phantom, the water loss after 10 days was lower in these two phantoms, which resulted in a more stable F/W-ratio over time. Although the difference between the F/W-ratio of the tumor phantom material between day 1 and day 10 in Gelatin-PVA and Gelatin-TG was significant with one star (*: p-value < 0.05), there is still a clear threshold between the F/W-ratio of the Tumor and Gland/Adipose layer, which enables the correct tissue classification using DRS. Based on the results of this research, the Gelatin-PVA and Gelatin-TG phantom can be still used for the intended application, even after 10 days after the production. Although using PVA and TG could increase the stability of the TMM material, the increased scattering of the TMM due to their presence can negatively affect their applicability for our application. However, using a more robust stirring system such as syndicators or powerful kitchen blenders instead of the magnetic stirrer can help for having a more homogeneous blend with finer particles especially for the TG phantom which can result in lower reduced scattering numbers [36].

Biomedical Optics EXPRESS

The pure lard which was used in this research contained no additives, while some lards that are available commercially may contain additives such as antioxidants that might alter the characteristics (optical, electrosurgery effect or other properties such as stability over time) of the final product [101]. The composition of the lard (percentage of each fatty acid) can vary depending on the animal's diet and the anatomical source of the lard. It has been shown that different components of the fatty acids have only a slight effect on the near-infrared absorption profile of the materials [40,102]. Furthermore, although during the production of the TMMs, lard from different batches (all batches were from the same butcher and animal organ but from different purchases) were used, no significant differences were seen between the optical profile (Fig. 3, 4 and 5) or fat-water content (Fig. 6) of the three replicates of each phantom (phantoms with same compositions). Nevertheless, further studies should be carried out to examine the effect of the lard's source on the final properties of the TMMs.

The TMM production method developed in this study can be used to produce materials with adjustable optical properties based on water and fat. The development of such methods and TMMs requires performing many experiments, which can lead to the use of large quantities of raw materials. Moreover, one of the aims of this research was to produce cost-efficient TMMs since the final products are intended to be used during electrosurgery, which results in the destruction of the phantom. Therefore, during the development of the TMMs, food-grade agar and gelatin were used to reduce the costs of the final product and produce a more cost-effective phantom recipe. Further studies can be done to comprehend the effect of using different agar or gelatin on the properties of the TMMs. The use of high quality and precisely processed agar and gelatin from scientific suppliers such as Sigma-Aldrich (Sigma-Aldrich, United States) in further studies may result in more reliable and reproducible phantoms, which in turn increases the costs of the final product.

Finally, the phantom materials were used to form anatomically-relevant breast phantoms for assessing breast imaging systems such as DRS. Moreover, the similar color and texture of the layers would make it difficult to detect the tumor borders surrounded with either Adipose or Gland TMMs, same as the situation that surgeons deal with during breast conserving surgery. The silicone layer, which could easily be removed from the phantom, was mainly used to ease the production process of the phantom and represent the appearance of the skin. No optical or any other characterization was done on this layer.

Although the application of DRS in the detection of breast tumors has been studied vastly, the capability of DRS in real-time detection of the tumor border, while moving the probe along the different layers of the breast tissue during the electrosurgery, has not yet been fully researched. Phantom studies can accelerate the adaptation of the DRS into clinical practice. In future studies, incisions in these anthropomorphic breast phantoms containing tumors can be made with the aim of simulating the intraoperative use of the DRS probe and electrosurgical knife in the detection and extraction of the tumors. The tumors containing Barium sulfate are clearly visible in the X-ray images, which enables to study of the performance of the intraoperative margin detection system after performing a BCS on the phantom. It is important to point out that in developing the TMMs, no action has been taken for quantitative simulation of the mechanical properties of the tissue. Although the application of hydrogel-based TMMs made it possible to develop soft phantoms, further studies and research are required to characterize and modify the mechanical properties of the phantoms for more quantitative simulation of breast tissue.

Table 3 summarizes the pros and cons of each developed TMMs for the intended application in this paper. While each TMMs developed in this research has its advantages over other phantoms, based on the results of this research and the discussed points, Agar phantom and Gelatin-TG phantom can better fulfil the requirements mentioned earlier and can be useful in applications that include optical measurements and electrosurgery.

Biomedical Optics EXPRESS

Table 3. Summarizing the pros and cons of each tissue mimicking phantom material.

Phantom	Pros	Cons
Agar	DRS spectra similar to the human breast tissue	No burning effect during electrosurgery unlike tissue
	closely simulating the absorption and scattering profile of the human breast tissue in NIR wavelength range	Low stability of optical properties after 10 days of storage
	No excessive melting during electrosurgery	
Gelatin	DRS spectra similar to the human breast tissue	Excessive melting during electrosurgery
	Closely simulating the scattering profile of the human breast tissue in NIR wavelength range	Low stability of optical properties after 10 days of storage
	Ease of manufacturing process	
Gelatin-PVA	DRS spectra similar to the human breast tissue	Melting during electrosurgery (rather than burning)
	High stability of optical properties after 10 days of storage	Higher reduced scattering coefficients due to the use of PVA
		Complicated manufacturing process
Gelatin-TGA	DRS spectra similar to the human breast tissue	High stability of optical properties after 10 days of storage
	Higher reduced scattering coefficients due to the use of TG	
	Tissue-like electrosurgery effect	

An ideal phantom intended to be used in assessing intraoperative tumor margin detection techniques, requires to be electrically conductive, since in most cancer surgeries, such as BCS (lumpectomy) and liver cancer, the electrosurgical knives will be used to cut out malignant tissue. However, developing such a phantom material meant for both applications (assessing the tumor detection technique while enabling electrosurgery) have not sufficiently been explored yet. To the best of our knowledge, this is the first fat-water based breast phantom used for optical measurement in the range of 1000–1600 nm which is also intended for electrosurgery. Hence, it seems there is still room for additional research regarding the production of such phantom materials. These phantom materials should have features that enable realistic simulation of the workflow during surgery/diagnosis either to validate, optimize and calibrate the margin detection technique or to train the medical residents and surgeons, as close as possible to reality.

As mentioned before, developing a physiologically relevant breast phantom representing the fat and water content of breast tissue is essential to evaluate the performance of the spectral imaging system in estimating the constituents of breast tissue. The results of this research show that using fat-water based TMMs, enable the simulation of human breast tissue's absorption and reduced scattering coefficient closely. Additionally, these type of phantoms can be used to assess other types of imaging systems that aim to measure the fat and water content of breast tissue for diagnostic or therapeutic purposes. For instance, these fat-water phantoms can be used for the assessment of X-ray and MRI imaging systems in the evaluation of the breast density, detection of lesions [69,103–105], or the assessment of Microwave imaging systems [60–62,64–66], or hybrid imaging techniques [67], or the assessment of therapeutic systems such as pulsed electric field [106].

5. Conclusion

In this study, tissue-mimicking materials with tunable optical properties were developed mainly based on water and porcine fat (lard). The developed phantom materials were produced in such a

Biomedical Optics EXPRESS

way that they could be cut using electrosurgical instruments, and as a result, they can be used to simulate surgeries in which an electrosurgical knife is used to remove the tumors. These tissue-mimicking phantom materials can be used to simulate the performance of optical-based imaging systems in detecting the breast tumor before moving to clinical trials.

Funding. The Netherlands Organization for Health Research and Development (ZonMw) (104006002).

Disclosures. Authors affiliated to Delft University of Technology and Eindhoven University of Technology have no financial interests in any materials, equipment and subject matter, and have not received any payments from Philips. Only B.H.W.H with the Philips affiliation has a financial interests in the materials, equipment and subject matter, in the sense that he is employee of Philips. The system described in this article is a research prototype and not for commercial use.

Data availability. Data underlying the results presented in this paper are not publicly available at this time but may be obtained from the authors upon reasonable request.

References

1. E. R. Sauter, "Breast cancer prevention: current approaches and future directions," Eur. J. Breast Health **14**, 64–71 (2018).
2. C. E. DeSantis, J. Ma, M. M. Gaudet, L. A. Newman, K. D. Miller, A. Goding Sauer, A. Jemal, and R. L. Siegel, "Breast cancer statistics, 2019," CA Cancer J. Clin. **69**(6), 438–451 (2019).
3. C. Chiappa, F. Rovera, A. D. Corben, A. Fachinetti, V. De Berardinis, V. Marchionini, S. Rausei, L. Boni, G. Dionigi, and R. Dionigi, "Surgical margins in breast conservation," Int. J. Surg. **11**, S69–S72 (2013).
4. D. W. Shipp, E. A. Rakha, A. A. Koloydenko, R. D. Macmillan, I. O. Ellis, and I. Notingher, "Intra-operative spectroscopic assessment of surgical margins during breast conserving surgery," Breast Cancer Res. **20**(1), 69 (2018).
5. C. M. O'Kelly Priddy, V. A. Forte, and J. E. Lang, "The importance of surgical margins in breast cancer," J. Surg. Oncol. **113**(3), 256–263 (2016).
6. E. Sadot, B. G. Koerkamp, J. N. Leal, J. Shia, M. Gonen, P. J. Allen, R. P. DeMatteo, T. P. Kingham, N. Kemeny, and L. H. Blumgart, "Resection margin and survival in 2368 patients undergoing hepatic resection for metastatic colorectal cancer: surgical technique or biologic surrogate?" Ann. Surg. **262**(3), 476–485 (2015).
7. M. S. Moran, S. J. Schnitt, A. E. Giuliano, J. R. Harris, S. A. Khan, J. Horton, S. Klimberg, M. Chavez-MacGregor, G. Freedman, and N. Houssami, "Society of Surgical Oncology–American Society for Radiation Oncology consensus guideline on margins for breast-conserving surgery with whole-breast irradiation in stages I and II invasive breast cancer," Int. J. Radiat. Oncol. Biol. Phys. **88**(3), 553–564 (2014).
8. C. Reyna and S. M. DeSnyder, "Intraoperative margin assessment in breast cancer management," Surg. Oncol. Clin. **27**(1), 155–165 (2018).
9. M. Pilewskie and M. Morrow, "Extent and role of margin control for DCIS managed by breast-conserving surgery," in *Ductal Carcinoma In Situ and Microinvasive/borderline Breast Cancer* (Springer, 2015), pp. 67–83.
10. R. Jeevan, D. Cromwell, M. Trivella, G. Lawrence, O. Kearins, J. Pereira, C. Sheppard, C. Caddy, and J. Van Der Meulen, "Reoperation rates after breast conserving surgery for breast cancer among women in England: retrospective study of hospital episode statistics," BMJ **345**(jul12 2), e4505 (2012).
11. J. Landercasper, E. Whitacre, A. C. Degnim, and M. Al-Hamadani, "Reasons for re-excision after lumpectomy for breast cancer: insight from the American Society of Breast Surgeons Mastery SM database," Ann. Surg. Oncol **21**(10), 3185–3191 (2014).
12. H. M. Kuerer, B. D. Smith, M. Chavez-MacGregor, C. Albarracin, C. H. Barcenas, L. Santiago, M. E. Edgerton, G. M. Rauch, S. H. Giordano, and A. Sahin, "DCIS margins and breast conservation: MD Anderson Cancer Center multidisciplinary practice guidelines and outcomes," J. Cancer **8**(14), 2653–2662 (2017).
13. B. L. Murphy, J. C. Boughey, M. G. Keeney, A. E. Glasgow, J. M. Racz, G. L. Keeney, and E. B. Habermann, "Factors associated with positive margins in women undergoing breast conservation surgery," in *Mayo Clinic Proceedings*, (Elsevier, 2018), 429–435.
14. L. A. Newman and J. M. Bensenhaver, *Ductal Carcinoma In Situ and Microinvasive/borderline Breast Cancer* (Springer, 2015).
15. L. Jacobs, "Positive margins: the challenge continues for breast surgeons," Ann. Surg. Oncol **15**(5), 1271–1272 (2008).
16. R. J. Gray, B. A. Pockaj, E. Garvey, and S. Blair, "Intraoperative margin management in breast-conserving surgery: a systematic review of the literature," Ann. Surg. Oncol **25**(1), 18–27 (2018).
17. R. Nachabe, B. H. Hendriks, A. E. Desjardins, M. Van Der Voort, M. B. Van Der Mark, and H. J. Sterenborg, "Estimation of lipid and water concentrations in scattering media with diffuse optical spectroscopy from 900 to 1600 nm," J. Biomed. Opt. **15**(3), 037015 (2010).
18. R. Nachabé, B. H. Hendriks, M. van der Voort, A. E. Desjardins, and H. J. Sterenborg, "Estimation of biological chromophores using diffuse optical spectroscopy: benefit of extending the UV-VIS wavelength range to include 1000 to 1600 nm," Biomed. Opt. Express **1**(5), 1432–1442 (2010).

Biomedical Optics EXPRESS

19. T. M. Bydlon, R. Nachabé, N. Ramanujam, H. J. Sterenborg, and B. H. Hendriks, "Chromophore based analyses of steady-state diffuse reflectance spectroscopy: current status and perspectives for clinical adoption," J. Biophotonics **8**(1-2), 9–24 (2015).
20. L. L. de Boer, B. H. Hendriks, F. Van Duijnhoven, M.-J. T. V. Peeters-Baas, K. Van de Vijver, C. E. Loo, K. Jóźwiak, H. J. Sterenborg, and T. J. J. B. O. E. Ruers, "Using DRS during breast conserving surgery: identifying robust optical parameters and influence of inter-patient variation," Biomed. Opt. Express **7**(12), 5188–5200 (2016).
21. L. De Boer, B. Molenkamp, T. Bydlon, B. Hendriks, J. Wesseling, H. Sterenborg, and T. J. Ruers, "Fat/water ratios measured with diffuse reflectance spectroscopy to detect breast tumor boundaries," Breast Cancer Res Treat **152**(3), 509–518 (2015).
22. L. L. de Boer, *Detecting breast cancer tissue with diffuse reflectance spectroscopy* (University of Twente, Enschede, 2019), p. 218.
23. R. Nachabe, B. H. Hendriks, G. W. Lucassen, M. van der Voort, D. J. Evers, E. J. Rutgers, M.-J. V. Peeters, J. A. Van der Hage, H. S. Oldenburg, and T. Ruers, "Diagnosis of breast cancer using diffuse optical spectroscopy from 500 to 1600 nm: comparison of classification methods," J. Biomed. Opt. **16**(8), 087010 (2011).
24. L. L. De Boer, T. M. Bydlon, F. Van Duijnhoven, M.-J. T. V. Peeters, C. E. Loo, G. A. Winter-Warnars, J. Sanders, H. J. Sterenborg, B. H. Hendriks, and T. J. Ruers, "Towards the use of diffuse reflectance spectroscopy for real-time in vivo detection of breast cancer during surgery," J. Transl. Med. **16**(1), 367 (2018).
25. T. M. Bydlon, S. A. Kennedy, L. M. Richards, J. Q. Brown, B. Yu, M. K. Junker, J. Gallagher, J. Geradts, L. G. Wilke, and N. Ramanujam, "Performance metrics of an optical spectral imaging system for intra-operative assessment of breast tumor margins," Opt. Express **18**(8), 8058–8076 (2010).
26. S. Kennedy, J. Geradts, T. Bydlon, J. Q. Brown, J. Gallagher, M. Junker, W. Barry, N. Ramanujam, and L. Wilke, "Optical breast cancer margin assessment: an observational study of the effects of tissue heterogeneity on optical contrast," Breast Cancer Res. **12**(6), R91–13 (2010).
27. L. L. de Boer, J. W. Spliethoff, H. J. Sterenborg, and T. J. Ruers, "in vivo optical spectral tissue sensing—how to go from research to routine clinical application?" Lasers Med. Sci. **32**(3), 711–719 (2017).
28. J. W. Spliethoff, L. L. de Boer, M. A. Meier, W. Prevoo, J. de Jong, K. Kuhlmann, T. M. Bydlon, H. J. Sterenborg, B. H. Hendriks, and T. J. Ruers, "In vivo characterization of colorectal metastases in human liver using diffuse reflectance spectroscopy: toward guidance in oncological procedures," J. Biomed. Opt. **21**(9), 097004 (2016).
29. J. Spliethof, *Spectral tissue sensing for guidance and monitoring in oncological procedures* (Universiteit Twente, Enschede, 2015), p. 194.
30. A. Keller, P. Bialecki, T. J. Wilhelm, and M. K. Vetter, "Diffuse reflectance spectroscopy of human liver tumor specimens-towards a tissue differentiating optical biopsy needle using light emitting diodes," Biomed. Opt. Express **9**(3), 1069–1081 (2018).
31. M. W. Adank, J. C. Fleischer, J. Dankelman, and B. H. W. Hendriks, "Real-time oncological guidance using diffuse reflectance spectroscopy in electrosurgery: the effect of coagulation on tissue discrimination," J. Biomed. Opt. **23**(11), 1 (2018).
32. S. A. Amiri, P. van Berckel, J. Dankelman, and B. H. Hendriks, "Electrosurgical knife equipped with diffused reflectance spectroscopy sensing for tumor margin detection during breast conserving surgery: a phantom study," in *Advanced Biomedical and Clinical Diagnostic and Surgical Guidance Systems XIX*, (International Society for Optics and Photonics, 2021), 1163110.
33. S. A. Amiri, C. M. Van Gent, J. Dankelman, and B. H. Hendriks, "Intraoperative tumor margin assessment using diffuse reflectance spectroscopy: the effect of electrosurgery on tissue discrimination using ex vivo animal tissue models," Biomed. Opt. Express **11**(5), 2402–2415 (2020).
34. A. E. Cerussi, R. Warren, B. Hill, D. Roblyer, A. Leproux, A. F. Durkin, T. D. O'Sullivan, S. Keene, H. Haghany, and T. Quang, "Tissue phantoms in multicenter clinical trials for diffuse optical technologies," Biomed. Opt. Express **3**(5), 966–971 (2012).
35. B. W. Pogue and M. S. Patterson, "Review of tissue simulating phantoms for optical spectroscopy, imaging and dosimetry," J. Biomed. Opt. **11**(4), 041102 (2006).
36. E. Ohmae, N. Yoshizawa, K. Yoshimoto, M. Hayashi, H. Wada, T. Mimura, H. Suzuki, S. Homma, N. Suzuki, and H. Ogura, "Stable tissue-simulating phantoms with various water and lipid contents for diffuse optical spectroscopy," Biomed. Opt. Express **9**(11), 5792–5808 (2018).
37. R. Pleijhuis, G. Langhout, W. Helfrich, G. Themelis, A. Sarantopoulos, L. Crane, N. Harlaar, J. De Jong, V. Ntziachristos, and G. Van Dam, "Near-infrared fluorescence (NIRF) imaging in breast-conserving surgery: assessing intraoperative techniques in tissue-simulating breast phantoms," Eur J Surg Oncol **37**(1), 32–39 (2011).
38. M. Anastasopoulou, M. Koch, D. Gorpas, A. Karlas, U. Klemm, P. B. Garcia-Allende, and V. Ntziachristos, "Comprehensive phantom for interventional fluorescence molecular imaging," J. Biomed. Opt. **21**(9), 091309 (2016).
39. G. Lamouche, B. F. Kennedy, K. M. Kennedy, C.-E. Bisaillon, A. Curatolo, G. Campbell, V. Pazos, and D. D. Sampson, "Review of tissue simulating phantoms with controllable optical, mechanical and structural properties for use in optical coherence tomography," Biomed. Opt. Express **3**(6), 1381–1398 (2012).
40. K. E. Michaelsen, V. Krishnaswamy, A. Shenoy, E. Jordan, B. W. Pogue, and K. D. Paulsen, "Anthropomorphic breast phantoms with physiological water, lipid, and hemoglobin content for near-infrared spectral tomography," J. Biomed. Opt. **19**(2), 026012 (2014).

Biomedical Optics EXPRESS

41. N. Ukhrowiyah, D. Hikmawat, M. Yasin, and R. Yuni, "Fabrication and characterization of breast phantom based on gelatin-glycerin-tio2 for a continuous-wave diffuse optical tomography," MJS **38**, 53–65 (2019).
42. W. C. Vogt, C. Jia, K. A. Wear, B. S. Garra, and T. J. Pfefer, "Biologically relevant photoacoustic imaging phantoms with tunable optical and acoustic properties," J. Biomed. Opt. **21**(10), 101405 (2016).
43. M. Dantuma, R. van Dommelen, and S. Manohar, "Semi-anthropomorphic photoacoustic breast phantom," Biomed. Opt. Express **10**(11), 5921–5939 (2019).
44. S. Merritt, G. Gulsen, G. Chiou, Y. Chu, C. Deng, A. E. Cerussi, A. J. Durkin, B. J. Tromberg, and O. Nalcioglu, "Comparison of water and lipid content measurements using diffuse optical spectroscopy and MRI in emulsion phantoms," Technol Cancer Res. **2**(6), 563–569 (2003).
45. L. C. Cabrelli, P. I. Pelissari, A. M. Deana, A. A. Carneiro, and T. Z. Pavan, "Stable phantom materials for ultrasound and optical imaging," Phys. Med. Biol. **62**(2), 432–447 (2017).
46. A. Taheri, P. Mansoori, L. F. Sandoval, S. R. Feldman, D. Pearce, and P. M. Williford, "Electrosurgery: part I. Basics and principles," J Am Acad Dermatol **70**(4), 591.e1 (2014).
47. M. G. Munro, "Fundamentals of electrosurgery part I: principles of radiofrequency energy for surgery," in *The SAGES Manual on the Fundamental Use of Surgical Energy (FUSE)* (Springer, 2012), pp. 15–59.
48. I. Alkatout, T. Schollmeyer, N. A. Hawaldar, N. Sharma, and L. Mettler, "Principles and safety measures of electrosurgery in laparoscopy," JSLS **16**(1), 130–139 (2012).
49. J. C. Hebden, B. D. Price, A. P. Gibson, and G. Royle, "A soft deformable tissue-equivalent phantom for diffuse optical tomography," Phys. Med. Biol. **51**(21), 5581–5590 (2006).
50. P. Li, Z. Yang, and S. Jiang, "Tissue mimicking materials in image-guided needle-based interventions: A review," Mater. Sci. Eng. C **93**, 1116–1131 (2018).
51. F. Ayers, A. Grant, D. Kuo, D. J. Cuccia, and A. J. Durkin, "Fabrication and characterization of silicone-based tissue phantoms with tunable optical properties in the visible and near infrared domain," in *Design and Performance Validation of Phantoms Used in Conjunction with Optical Measurements of Tissue* (International Society for Optics and Photonics, 2008), 687007.
52. G. T. Kennedy, G. R. Lentsch, B. Trieu, A. Ponticorvo, R. B. Saager, and A. J. Durkin, "Solid tissue simulating phantoms having absorption at 970 nm for diffuse optics," J. Biomed. Opt. **22**(7), 076013 (2017).
53. J. Garrett and E. Fear, "A new breast phantom with a durable skin layer for microwave breast imaging," IEEE Transactions on Antennas Propagation **63**(4), 1693–1700 (2015).
54. A. I. Chen, M. L. Balter, M. I. Chen, D. Gross, S. K. Alam, T. J. Maguire, and M. L. Yarmush, "Multilayered tissue mimicking skin and vessel phantoms with tunable mechanical, optical, and acoustic properties," Med. Phys. **43**(6Part1), 3117–3131 (2016).
55. S. Srinivasan, C. M. Carpenter, H. R. Ghadyani, S. J. Taka, P. A. Kaufman, W. A. Wells, B. W. Pogue, and K. D. Paulsen, "Image guided near-infrared spectroscopy of breast tissue in vivo using boundary element method," J. Biomed. Opt. **15**(6), 061703 (2010).
56. G. Menikou and C. Damianou, "Acoustic and thermal characterization of agar based phantoms used for evaluating focused ultrasound exposures," J. Ther. Ultrasound **5**(1), 14 (2017).
57. M. A. Kandadai, J. L. Raymond, and G. J. Shaw, "Comparison of electrical conductivities of various brain phantom gels: Developing a 'brain gel model'," Mater. Sci. Eng. C **32**(8), 2664–2667 (2012).
58. G. Quarto, A. Pifferi, I. Bargigia, A. Farina, R. Cubeddu, and P. Taroni, "Comparison of organic phantom recipes and characterization by time-resolved diffuse optical spectroscopy," in *European Conference on Biomedical Optics*, (Optical Society of America, 2013), 879905.
59. E. C. Bush, A. Gifford, C. L. Coolbaugh, T. F. Towse, B. M. Damon, and E. B. Welch, "Fat-water phantoms for magnetic resonance imaging validation: a flexible and scalable protocol," JoVE **139**, e57704 (2018).
60. M. O'Halloran, S. Lohfeld, G. Ruvio, J. Browne, F. Krewer, C. Ribeiro, V. I. Pita, R. Conceicao, E. Jones, and M. Glavin, "Development of anatomically and dielectrically accurate breast phantoms for microwave imaging applications," in *Radar Sensor Technology XVIII*, (International Society for Optics and Photonics, 2014), 90770Y.
61. N. Joachimowicz, C. Conessa, T. Henriksson, and B. Duchêne, "Breast phantoms for microwave imaging," IEEE Antennas Wirel. Propag. Lett. **13**, 1333–1336 (2014).
62. M. Ostadrahimi, R. Reopelle, S. Noghanian, S. Pistorius, A. Vahedi, and F. Safari, "A heterogeneous breast phantom for microwave breast imaging," in *2009 Annual International Conference of the IEEE Engineering in Medicine and Biology Society* (IEEE, 2009), 2727–2730.
63. M. Miyakawa, S. Takata, and K. Inotsume, "Development of non-uniform breast phantom and its microwave imaging for tumor detection by CP-MCT," in *2009 Annual International Conference of the IEEE Engineering in Medicine and Biology Society* (IEEE, 2009), 2723–2726.
64. C. Hahn and S. Noghanian, "Heterogeneous breast phantom development for microwave imaging using regression models," Int. J. Biomed. Imaging **2012**, 1–12 (2012).
65. J. C. Y. Lai, C. B. Soh, E. Gunawan, and K. S. Low, "Homogeneous and heterogeneous breast phantoms for ultra-wideband microwave imaging applications," Prog. Electromagn. Res. **100**, 397–415 (2010).
66. E. Porter, J. Fakhoury, R. Oprisor, M. Coates, and M. Popović, "Improved tissue phantoms for experimental validation of microwave breast cancer detection," in *Proceedings of the fourth European conference on antennas and propagation* (IEEE, 2010), 1–5.

Biomedical Optics EXPRESS

67. B. Henin, A. Abbosh, and W. Al Abdulla, "Electro-biomechanical breast phantom for hybrid breast imaging," in *2015 International Symposium on Antennas and Propagation (ISAP)* (IEEE, 2015), 1–3.
68. I. E. Khuda, "A comprehensive review on design and development of human breast phantoms for ultra-wide band breast cancer imaging systems," EJ **21**(3), 183–206 (2017).
69. M. Freed, J. A. de Zwart, J. T. Loud, R. H. El Khouli, K. J. Myers, M. H. Greene, J. H. Duyn, and A. Badano, "An anthropomorphic phantom for quantitative evaluation of breast MRI," Med. Phys. **38**(2), 743–753 (2011).
70. J. Meshram, V. Koli, M. Phadatare, and S. Pawar, "Anti-microbial surfaces: An approach for deposition of ZnO nanoparticles on PVA-Gelatin composite film by screen printing technique," Mater. Sci. Eng. C **73**, 257–266 (2017).
71. P. N. Charron, T. A. Braddish, and R. A. Oldinski, "PVA-gelatin hydrogels formed using combined theta-gel and cryo-gel fabrication techniques," J. Mech. Behav. Biomed. Mater. **92**, 90–96 (2019).
72. Y. Liu, L. M. Geever, J. E. Kennedy, C. L. Higginbotham, P. A. Cahill, and G. B. McGuinness, "Thermal behavior and mechanical properties of physically crosslinked PVA/Gelatin hydrogels," J. Mech. Behav. Biomed. Mater. **3**(2), 203–209 (2010).
73. M. A. Anugrah, S. Ilyas, and D. Tahir, "Gelatin/Poly (vinyl alcohol)/Inorganic filler composites for phantom breasts," Mater. Chem. Phys. **262**, 124333 (2021).
74. A. Thangprasert, C. Tansakul, N. Thuaksubun, and J. Meesane, "Mimicked hybrid hydrogel based on gelatin/PVA for tissue engineering in subchondral bone interface for osteoarthritis surgery," Mater. Des. **183**, 108113 (2019).
75. A. Ito, A. Mase, Y. Takizawa, M. Shinkai, H. Honda, K.-I. Hata, M. Ueda, and T. Kobayashi, "Transglutaminase-mediated gelatin matrices incorporating cell adhesion factors as a biomaterial for tissue engineering," J. Biosci. Bioeng. **95**(2), 196–199 (2003).
76. M. K. McDermott, T. Chen, C. M. Williams, K. M. Markley, and G. F. Payne, "Mechanical properties of biomimetic tissue adhesive based on the microbial transglutaminase-catalyzed crosslinking of gelatin," Biomacromolecules **5**(4), 1270–1279 (2004).
77. L. T. Lim, Y. Mine, and M. Tung, "Barrier and tensile properties of transglutaminase cross-linked gelatin films as affected by relative humidity, temperature, and glycerol content," J. Food Sci. **64**(4), 616–622 (1999).
78. S. A. Irvine, A. Agrawal, B. H. Lee, H. Y. Chua, K. Y. Low, B. C. Lau, M. Machluf, and S. Venkatraman, "Printing cell-laden gelatin constructs by free-form fabrication and enzymatic protein crosslinking," Biomed. Microdevices **17**(1), 16 (2015).
79. L. M. Bellan, M. Pearsall, D. M. Cropek, and R. Langer, "A 3D interconnected microchannel network formed in gelatin by sacrificial shellac microfibers," Adv. Mater **24**(38), 5187–5191 (2012).
80. M. K. George, J. E. Tierney, A. C. Luchies, K. A. Ozgun, S. Faley, L. M. Bellan, and B. C. Byram, "Perfusion flow phantoms with randomly oriented microchannels," in *Medical Imaging 2018: Ultrasonic Imaging and Tomography* (International Society for Optics and Photonics, 2018), 1058006.
81. R. Nachabe, B. H. Hendriks, and H. Sterenborg, "Determination of water and lipid concentrations by diffuse optical spectroscopy in lipid emulsions in the wavelength range of 1000 to 1500 nm," in *Biomedical Optics*, (Optical Society of America, 2010), BTuD88.
82. R. K. Chen and A. Shih, "Multi-modality gellan gum-based tissue-mimicking phantom with targeted mechanical, electrical, and thermal properties," Phys. Med. Biol. **58**(16), 5511–5525 (2013).
83. S. A. Solazzo, Z. Liu, S. M. Lobo, M. Ahmed, A. U. Hines-Peralta, R. E. Lenkinski, and S. N. J. R. Goldberg, "Radiofrequency ablation: importance of background tissue electrical conductivity—an agar phantom and computer modeling study," Radiology **236**(2), 495–502 (2005).
84. C. Ianniello, J. A. de Zwart, Q. Duan, C. M. Deniz, L. Alon, J. S. Lee, R. Lattanzi, and R. Brown, "Synthesized tissue-equivalent dielectric phantoms using salt and polyvinylpyrrolidone solutions," Magn. Reson. Med **80**(1), 413–419 (2018).
85. V. G. Sirtoli, K. Morcelles, and P. Bertemes-Filho, "Electrical properties of phantoms for mimicking breast tissue," in *2017 39th Annual International Conference of the IEEE Engineering in Medicine and Biology Society (EMBC)*, (IEEE, 2017), 157–160.
86. C. K. Chou, G. W. Chen, A. W. Guy, and K. H. Luk, "Formulas for preparing phantom muscle tissue at various radiofrequencies," Bioelectromagnetics **5**, 435–441 (1984).
87. G. Fiaschetti, J. Browne, M. Cavagnaro, L. Farina, and G. Ruvio, "Tissue mimicking materials for multi-modality breast phantoms," in *2018 2nd URSI Atlantic Radio Science Meeting (AT-RASC)* (IEEE, 2018), 1–6.
88. T. J. Farrell, M. S. Patterson, and B. Wilson, "A diffusion theory model of spatially resolved, steady-state diffuse reflectance for the noninvasive determination of tissue optical properties in vivo," Med. Phys. **19**(4), 879–888 (1992).
89. R. Nachabé, D. J. Evers, B. H. Hendriks, G. W. Lucassen, M. van der Voort, J. Wesseling, and T. J. Ruers, "Effect of bile absorption coefficients on the estimation of liver tissue optical properties and related implications in discriminating healthy and tumorous samples," Biomed. Opt. Express **2**(3), 600–614 (2011).
90. R. Nachabé, Diagnosis with near infrared spectroscopy during minimally invasive procedures (2012), p. 232.
91. D. J. Evers, R. Nachabe, M.-J. V. Peeters, J. A. van der Hage, H. S. Oldenburg, E. J. Rutgers, G. W. Lucassen, B. H. Hendriks, J. Wesseling, and T. J. Ruers, "Diffuse reflectance spectroscopy: towards clinical application in breast cancer," Breast Cancer Res Treat **137**(1), 155–165 (2013).
92. M. Dantuma, "Dataset 1.STL," figshare (2019). https://doi.org/10.6084/m9.figshare.9911747.v1.
93. M. Dantuma, "Dataset 2.STL," figshare (2019). https://doi.org/10.6084/m9.figshare.9911750.v1

Biomedical Optics EXPRESS

94. P. Taroni, G. Quarto, A. Pifferi, F. Abbate, N. Balestreri, S. Menna, E. Cassano, and R. Cubeddu, "Breast tissue composition and its dependence on demographic risk factors for breast cancer: non-invasive assessment by time domain diffuse optical spectroscopy," PLoS ONE **10**(6), e0128941 (2015).
95. N. Yoshizawa, Y. Ueda, T. Mimura, E. Ohmae, K. Yoshimoto, H. Wada, H. Ogura, and H. Sakahara, "Factors affecting measurement of optic parameters by time-resolved near-infrared spectroscopy in breast cancer," J. Biomed. Opt. **23**(02), 1 (2018).
96. A. H. Poh, M. F. Jamaludin, I. A. Fadzallah, N. M. J. Nik Ibrahim, F. Yusof, F. R. M. Adikan, and M. J. J. O. N. I. S Moghavvemi, "Diffuse reflectance spectroscopic analysis of barium sulfate as a reflection standard within 173–2500 nm: From pure to sintered form," **27**, 393–401 (2019).
97. M. Islam, M. Mahmud, M. T. Islam, S. Kibria, and M. Samsuzzaman, "A low cost and portable microwave imaging system for breast tumor detection using UWB directional antenna array," Sci. Rep. **9**(1), 15491 (2019).
98. G. Anand, A. Lowe, and A. Al-Jumaily, "Tissue phantoms to mimic the dielectric properties of human forearm section for multi-frequency bioimpedance analysis at low frequencies," Mater. Sci. Eng. C **96**, 496–508 (2019).
99. Y. Liu, R. Weng, W. Wang, X. Wei, J. Li, X. Chen, Y. Liu, F. Lu, and Y. Li, "Tunable physical and mechanical properties of gelatin hydrogel after transglutaminase crosslinking on two gelatin types," Int. J. Biol. Macromol. **162**, 405–413 (2020).
100. Y. Wang, A. Liu, R. Ye, W. Wang, and X. Li, "Transglutaminase-induced crosslinking of gelatin–calcium carbonate composite films," Food Chem. **166**, 414–422 (2015).
101. L. Atarés, R. Pérez-Masiá, and A. Chiralt, "The role of some antioxidants in the HPMC film properties and lipid protection in coated toasted almonds," J. Food Eng. **104**(4), 649–656 (2011).
102. C.-L. Tsai, J.-C. Chen, W.-J. J. o, and M. Wang, "Near-infrared absorption property of biological soft tissue constituents," J. Med. Biol. Eng. **21**, 7–14 (2001).
103. J. Byng, J. Mainprize, and M. Yaffe, "X-ray characterization of breast phantom materials," Phys. Med. Biol. **43**(5), 1367–1377 (1998).
104. G. J. Wengert, K. Pinker, T. H. Helbich, W. D. Vogl, S. M. Spijker, H. Bickel, S. H. Polanec, and P. A. Baltzer, "Accuracy of fully automated, quantitative, volumetric measurement of the amount of fibroglandular breast tissue using MRI: correlation with anthropomorphic breast phantoms," NMR Biomed. **30**(6), e3705 (2017).
105. M. Freed, A. Badal, R. J. Jennings, H. de las Heras, K. J. Myers, and A. Badano, "X-ray properties of an anthropomorphic breast phantom for MRI and x-ray imaging," Phys. Med. Biol. **56**(12), 3513–3533 (2011).
106. S. Poompavai and V. G. Sree, "Dielectric property measurement of breast—Tumor phantom model under pulsed electric field treatment," IEEE Trans. Radiat. Plasma Med. Sci. **2**(6), 608–617 (2018).